

June 8, 2021

# Azimuthal angle correlations in hadron-nucleus scattering: enhanced diagrams

---

Eugene Levin <sup>a,b</sup> and Sebastian Tapia <sup>a</sup>

<sup>a</sup> *Departamento de Física, Universidad Técnica Federico Santa María and Centro Científico-Tecnológico de Valparaíso, Casilla 110-V, Valparaíso, Chile*

<sup>b</sup> *Department of Particle Physics, School of Physics and Astronomy, Tel Aviv University, Tel Aviv, 69978, Israel*

ABSTRACT: In this paper we calculate the contribution to rapidity and angular correlations of the first Pomeron loop diagram in the dense partonic environment. This diagram is expected to give the largest contribution to the density variation mechanism of the angular correlations. We show that this diagrams leads to sizable contributions to the rapidity correlation functions of the order of  $\sigma_{in}/(\pi R^2)$  where  $\sigma_{in}$  is the inelastic cross section and  $R$  is the size of the typical dipole inside the proton saturation scale. Therefore, the correlations do not depend on the saturation scale. We demonstrated that density variation mechanism does not lead to suppression of the angular dependance of the double inclusive cross section generating the coefficient in front of  $\cos^2\varphi$  in  $A^{1/3}$  larger in the case of hadron-nucleus collision than in hadron-hadron interaction. The angular correlations are suppressed in comparison with the rapidity ones but only due to large multiplicity of the produced gluons. We consider this paper as the first attempt of quantitative description of the density variation mechanism in CGC/saturation approach.

KEYWORDS: BFKL Pomeron, saturation/Color Glass Condensate approach, BFKL Pomeron calculus, angular and correlations in saturation approach .

PACS: 12.38-t, 12.38.Cy, 12.38.Lg, 13.60.Hd, 24.85.+p, 25.30.Hm

---

## Contents

<b>1. Introduction</b>	<b>2</b>
<b>2. Correlations: first enhanced diagrams contribution</b>	<b>4</b>
2.1 The BFKL Pomeron: generalities	5
2.2 Inclusive production in dipole-dipole scattering: the BFKL Pomeron contribution	8
2.3 Inclusive production in dipole-dipole scattering: non-linear equation	9
2.4 Rapidity correlations	10
2.5 Azimuthal angle correlations	18
<b>3. The first enhanced diagram in the saturation environment</b>	<b>25</b>
3.1 Equation for Pomeron Green's function	25
3.2 Solutions	27
3.2.1 The toy model	27
3.2.2 Equations in the momentum representation	28
3.2.3 Solution to the equations	29
3.2.4 Solution to the equation in the vicinity of the saturation scale	31
<b>4. Enhanced diagrams: correlations in hadron-nucleus scattering</b>	<b>31</b>
<b>5. Conclusions</b>	<b>34</b>
<b>6. Acknowledgements</b>	<b>35</b>

## 1. Introduction

One of the most intriguing experimental observation made at the LHC and RHIC, is the same pattern of the azimuthal angle correlations in three type of the interactions: hadron-hadron, hadron-nucleus and nucleus-nucleus collisions. In all three reactions the correlations are observed between two charged hadrons which are separated by the large values of rapidity in the events with large density of the produced particles [1–7]. We believe that these experiments provide a strong evidence that the underlying physics is the same for all three reactions and it is related the partonic state with high density that has been produced at high energies in all three reactions. Due to causality arguments [8] two hadrons with large difference in rapidity between them could correlate only at the early stage of the collision and, therefore, we expect that the correlations between two particles with large rapidity difference (at least the correlations in rapidity) stem from the partonic state with large parton density. The parton (gluon) density is governed in QCD by the linear BFKL equation [9, 10] which is independent of the type of reaction and leads to the increase of the gluon density. The BFKL evolution describes the emission of gluons at high energy but do not take into account the possible annihilation processes at high energy that stop the density growth and manifest themselves in the gluon saturation [11] and in the appearance of the new scale: saturation momentum  $Q_s(x)$  (where  $x$  is the fraction of energy carried by the gluon) [11–14]. Such dense system of gluons is frequently referred to as the Color Glass Condensate (CGC). For the collision of dilute gluon system with the dense system (say for hadron-nucleus collisions) we can analyze CGC using the BK-JIMWLK approach [15–17] which provide us the equations for the non-linear evolution. However, for dilute-dilute scattering (say hadron-hadron collisions) and for dense-dense scattering (nucleus-nucleus scattering) we can base our approach to correlations on the analysis of large Pomeron loops contribution (see Ref. [18]).

Unlike the rapidity correlations at large values of the rapidity difference which stem from the initial state interactions, the azimuthal angle correlations can be originated by collective flow in the final state [19]. Nevertheless, in this paper we would like to analyze the same mechanism for both correlations: the initial state interaction in the CGC phase of QCD. However, even in the framework of saturation/CGC approach we are not able propose the unique mechanism for the azimuthal angle correlations. At the moment we have three sources of the azimuthal angle correlation on the market:\* Bose enhancement in the wave function [21], local anisotropy [22, 23] and density variation [24, 25]. We cite only the restricted number of papers for each approach. A reader could find more references and more ideas on the origin of the correlation in the review paper of Refs. [23, 26–31].

The goal of this paper to study in more details the density variation mechanism proposed in Ref. [24]. In this approach both rapidity and azimuthal angle correlations stem from two gluons production from two parton showers. This production can be written using Mueller diagrams [32] (see Fig. 1). The difference between rapidity and azimuthal angle correlations is only in the form of the Mueller vertices in Fig. 1.

For rapidity correlations such vertex can be considered being independent on  $Q_T$  while for the azimuthal angle correlation this vertex is proportional to  $(\vec{Q}_T \cdot p_{1,\perp})^2$  or  $(\vec{Q}_T \cdot p_{2,\perp})^2$ . The integration over the

---

\*We use classification and terminology suggested in Ref. [20].

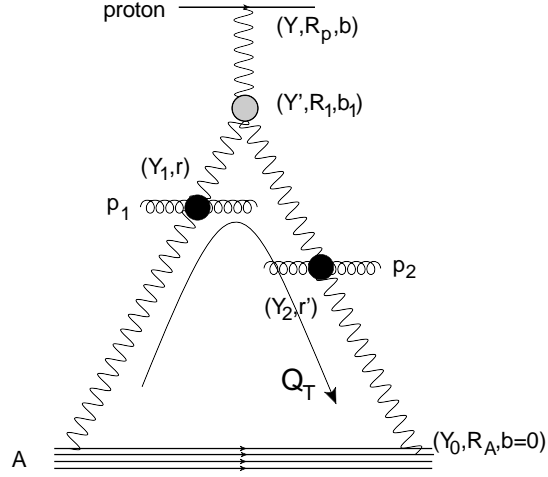


**Figure 1:** Mueller diagrams [32]: the first fan diagram for two particle correlation. Wavy lines denote the BFKL Pomerons. Helix lines show the gluons. Black blob stands for the Mueller vertex for inclusive production of gluon jet with the transverse momentum  $p_{\perp,1}$  ( $p_{\perp,2}$ ), respectively.

direction of  $\vec{Q}_T$  leads to the term  $(\vec{p}_{1,\perp} \cdot \vec{p}_{2,\perp})^2$  which is proportional to  $\cos 2\varphi$  resulting in the azimuthal angle correlations. The strength of the term  $\cos 2\varphi$  is proportional to  $\langle Q_T^2 \rangle^2$  where averaging is taken over the wave function of one parton shower which is described by the BFKL Pomeron. In other words since  $\vec{Q}_T = i\nabla_b$  where  $b$  is the impact factor for the scattering process the magnitude of the azimuthal angle correlation depends on the gradient of the parton density. As it is shown in Ref. [24] for hadron-nucleus scattering the diagram of Fig. 1 generates the following azimuthal angle correlations:

$$\begin{aligned}
 R(b, \varphi, Y_1, Y_2) &= \sigma_{in} \frac{d\sigma}{dY_1 dY_2 d^2p_{1\perp} dp_{2\perp}} \bigg/ \frac{d\sigma}{dY_1 d^2p_{1\perp}} \frac{d\sigma}{dY_2 dp_{2\perp}} - 1 \\
 &= p_{1\perp}^2 p_{2\perp}^2 2 \left( \langle \frac{1}{q^4} \rangle |_{\text{proton}} \right)^2 \nabla_b^2 \nabla_b^2 S_A^2(b) (2 + \cos 2\varphi)
 \end{aligned} \tag{1.1}$$

where

$$S_A(b) = \int dl \rho(l, b) \quad \text{with normalization} \quad \int d^2b S_A(b) = A \tag{1.2}$$

where  $\rho(l, b)$  is the nucleon density and  $l$  is the longitudinal coordinate.

One can see that Eq. (1.1) gives small correlations since  $\nabla^2 S_A(b) \propto 1/R_A^2$ . In other words the correlation turns out to be small since  $Q_T \approx 1/R_A$  in the diagram of Fig. 1. In this diagram the variation of the gluon density is reduced to the variation of the density of the nucleons in the nucleus which characterize by the large correlation length of the order of the nucleus radius. On the other hand, in the CGC phase of QCD the natural correlation length is of the order of  $1/Q_s \propto 1/A^{1/6}$  which translates to  $Q_T \approx Q_s$ . The diagrams, in which we can expect that  $Q_T$  will be about  $Q_s$ , are the enhanced diagrams<sup>†</sup>. The simplest

<sup>†</sup>The importance of enhanced diagram for the azimuthal angle correlations was noted first in Refs. [22, 24].

one is shown in Fig. 2. One can see without any detailed calculations that the typical value of  $Q_T$  will be equal to  $1/r$ ,  $1/R_1$  or  $1/R_2$ , all of which are not related to the radius of the nucleus.

In this paper we will calculate the simplest enhanced diagrams for the hadron-nucleus and hadron-hadron interactions and will try to understand the main features of this diagram which would affect the azimuthal angle correlations. In section 2 we introduce the main ingredients and calculate the first Pomeron loop diagram for the hadron-hadron interaction. We show that this calculation are quite different from the calculation of the same diagram but for its contribution to the total cross section. We discuss in details the integration over the loop momentum which leads to the same values of the dipole sizes in the triple Pomeron vertices. Section 3 is devoted to the calculation of Green's function of the BFKL Pomeron in the saturation environment. The equations are written and solved. In section 4 we summarize our calculations for hadron-nucleus scattering. In conclusions we present our main result and discussed their naturalness.

## 2. Correlations: first enhanced diagrams contribution

We start the analysis of the azimuthal angle correlation considering the first enhanced diagram, shown in Fig. 2. As we have discussed in the introduction we are looking for the mechanism of correlation based on large densities gradients [20, 24] and the enhanced diagrams lead to the gradients of the order of  $Q_s$ . Calculating the first loop diagram we wish to demonstrate this fact and to discuss the scale of the correlations.

The contribution of Fig. 2 to the double inclusive cross section for scattering of two dipole with the sizes  $R_p$  and  $R_A^\dagger$ , takes the form [35] (see Fig. 2 for notations):

$$\begin{aligned} \frac{p_{\perp,1}^2 p_{\perp,2}^2 d\sigma}{dY_1 dY_2 d^2 p_{\perp,1} d^2 p_{\perp,2}} &= \frac{4\pi^2 \bar{\alpha}_S^4}{N_c^2} \int d^2 b \int d^2 b_1 \int d^2 b_2 \int_{Y_1}^Y dY' \int_{Y_0}^{Y_2} dY'' \\ &\int \frac{d^2 R_1}{R_1^4} \int \frac{d^2 R_2}{R_2^4} N_{\mathcal{P}} \left( Y - Y'; R_p, R_1, \vec{b} - \vec{b}_1 \right) \int d^2 R'_1 \int d^2 R'_2 K \left( R_1, R'_1 \right) \\ &N_{\mathcal{P}}^{\text{incl}} \left( Y' - Y'', R'_1, R'_2, \vec{b}_1 - \vec{b}_2 | p_{\perp,1}, Y_1 \right) N_{\mathcal{P}}^{\text{incl}} \left( Y' - Y'', \vec{R}_1 - \vec{R}'_1, \vec{R}_2 - \vec{R}'_2, \vec{b}_1 - \vec{b}_2 | p_{\perp,2}, Y_2 \right) \\ &K \left( R_2, R'_2 \right) N_{\mathcal{P}} \left( Y'' - Y_0; R_2, R_A, \vec{b}_2 \right) \end{aligned} \quad (2.1)$$

where  $N_{\mathcal{P}} \left( Y; r_1, r_2, \vec{b} \right)$  is the amplitude of the dipole-dipole scattering with the dipole sizes  $r_1$  and  $r_2$ , at rapidity  $Y$  and at impact parameter  $b$  due to the exchange of the BFKL Pomeron [9, 10, 17].  $N_{\mathcal{P}}^{\text{incl}} \left( Y, r_1, r_2, \vec{b} | p_{\perp}, Y_1 \right)$  is the BFKL Pomeron contribution to the inclusive cross section of the gluon jet production with rapidity  $Y_1$  and transverse momentum  $p_{\perp}$  in the dipole-dipole scattering of two dipoles with the sizes  $r_1$  and  $r_2$  at rapidity  $Y$  and at impact parameters  $b$ . The triple Pomeron vertex  $K \left( r, r' \right)$  takes a familiar form:

$$K \left( r, r' \right) = \frac{r^2}{r'^2 \left( \vec{r} - \vec{r}' \right)^2} \quad (2.2)$$

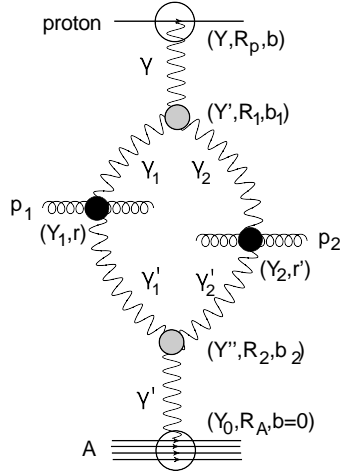


**Figure 2:** The first enhanced (loop) diagram for two particle correlation. Wavy lines denote the BFKL Pomeron. Helix lines show the gluons. Black blob stands for the Mueller vertex ( $a_P$ ) for inclusive production of gluon jet with the transverse momentum  $p_{\perp,1}$  ( $p_{\perp,2}$ ), respectively. The gray blobs show the triple Pomeron vertices ( $G_{3P}$ ). The vertices of interaction with the proton and the nucleus ( $g_p$  and  $g_A$ ) are shown by circles.

All ingredients of Eq. (2.1) we consider separately below, starting with  $N_{IP}$ .

## 2.1 The BFKL Pomeron: generalities

The general solution to the BFKL equation for the scattering amplitude of two dipoles with the sizes  $r_1$  and  $r_2$  has been derived in Ref. [10] and it takes the form

$$N_{IP}(r_1, r_2; Y, b) = \sum_{n=0}^{\infty} \int \frac{d\gamma}{2\pi i} \phi_{in}^{(n)}(\gamma; r_2) d^2 R_1 d^2 R_2 \delta(\vec{R}_1 - \vec{R}_2 - \vec{b}) e^{\omega(\gamma, n)Y} E^{\gamma, n}(r_1, R_1) E^{1-\gamma, n}(r_2, R_2) \quad (2.3)$$

with

$$\omega(\gamma, n) = \bar{\alpha}_S \chi(\gamma, n) = \bar{\alpha}_S (2\psi(1) - \psi(\gamma + |n|/2) - \psi(1 - \gamma + |n|/2)); \quad (2.4)$$

where  $\psi(\gamma) = d \ln \Gamma(\gamma) / d\gamma$  and  $\Gamma(\gamma)$  is Euler gamma function. Functions  $E^{n, \gamma}(\rho_{1a}, \rho_{2a})$  are given by the following equations.

$$E^{n, \gamma}(\rho_{1a}, \rho_{2a}) = \left( \frac{\rho_{12}}{\rho_{1a} \rho_{2a}} \right)^{1-\gamma+n/2} \left( \frac{\rho_{12}^*}{\rho_{1a}^* \rho_{2a}^*} \right)^{1-\gamma-n/2}, \quad (2.5)$$

In Eq. (2.5) we use the complex numbers to characterize the point on the plane

$$\rho_i = x_{i,1} + i x_{i,2}; \quad \rho_i^* = x_{i,1} - i x_{i,2} \quad (2.6)$$

where the indices 1 and 2 denote two transverse axes. Notice that

$$\rho_{12} \rho_{12}^* = r_i^2; \quad \rho_{1a} \rho_{1a}^* = \left( \vec{R}_i - \frac{1}{2} \vec{r}_i \right)^2 \quad \rho_{2a} \rho_{2a}^* = \left( \vec{R}_i + \frac{1}{2} \vec{r}_i \right)^2 \quad (2.7)$$

<sup>†</sup>We need to stipulate that  $R_A$  is not the radius of a nucleus but the size of the typical dipole inside the nucleus which is of the same order as  $R_p$ .

At large values of  $Y$  the main contribution stems from the first term with  $n = 0$ . For this term Eq. (2.5) can be re-written in the form

$$E^{\gamma,0}(r_i, R_i) = \left( \frac{r_i^2}{(\vec{R}_i + \frac{1}{2}\vec{r}_i)^2 (\vec{R}_i - \frac{1}{2}\vec{r}_i)^2} \right)^{1-\gamma}. \quad (2.8)$$

The integrals over  $R_1$  and  $R_2$  were taken in Refs. [10, 33] and at  $n = 0$  we have

$$\begin{aligned} H^\gamma(w, w^*) &\equiv \int d^2 R_1 E^{\gamma,0}(r_1, R_1) E^{1-\gamma,0}(r_2, \vec{R}_1 - \vec{b}) = \\ &\frac{(\gamma - \frac{1}{2})^2}{(\gamma(1-\gamma))^2} \left\{ b_\gamma w^\gamma w^{*\gamma} F(\gamma, \gamma, 2\gamma, w) F(\gamma, \gamma, 2\gamma, w^*) + \right. \\ &\left. b_{1-\gamma} w^{1-\gamma} w^{*1-\gamma} F(1-\gamma, 1-\gamma, 2-2\gamma, w) F(1-\gamma, 1-\gamma, 2-2\gamma, w^*) \right\} \end{aligned} \quad (2.9)$$

where  $F$  is hypergeometric function [34]. In Eq. (2.9)  $w w^*$  is equal to

$$w w^* = \frac{r_1^2 r_2^2}{\left(\vec{b} - \frac{1}{2}(\vec{r}_1 - \vec{r}_2)\right)^2 \left(\vec{b} + \frac{1}{2}(\vec{r}_1 - \vec{r}_2)\right)^2} \quad (2.10)$$

and  $b_\gamma$  is equal to

$$b_\gamma = \pi^3 2^{4(1/2-\gamma)} \frac{\Gamma(\gamma)}{\Gamma(1/2-\gamma)} \frac{\Gamma(1-\gamma)}{\Gamma(1/2+\gamma)}. \quad (2.11)$$

Finally, the solution at large  $Y$  takes the form

$$N_{\mathbb{P}}(r_1, r_2; Y, b) = \int \frac{d\gamma}{2\pi i} e^{\omega(\gamma,0)Y} H^\gamma(w, w^*) \quad (2.12)$$

In the vicinity of the saturation scale  $N_{\mathbb{P}}$  takes the form (see Refs. [36, 38])

$$\begin{aligned} N_{\mathbb{P}}(r_1, r_2; Y, b) &= \frac{(\gamma_{cr} - \frac{1}{2})^2}{\gamma_{cr}(1-\gamma_{cr})} b_{\gamma_{cr}} (w w^* e^{\kappa Y})^{1-\gamma_{cr}} \\ &= \frac{(\gamma_{cr} - \frac{1}{2})^2}{\gamma_{cr}(1-\gamma_{cr})} b_{\gamma_{cr}} \left( \left( \frac{r_1^2 r_2^2}{\left(\vec{b} - \frac{1}{2}(\vec{r}_1 - \vec{r}_2)\right)^2 \left(\vec{b} + \frac{1}{2}(\vec{r}_1 - \vec{r}_2)\right)^2} \right) e^{\bar{\alpha}_S \frac{\chi(\gamma_{cr})}{1-\gamma_{cr}} Y} \right)^{1-\gamma_{cr}} \end{aligned} \quad (2.13)$$

$$\xrightarrow{r_2 \gg r_1} \phi_0 \left( r_1^2 Q_s^2(r_2, b; Y) \right)^{1-\gamma_{cr}} \quad \text{with} \quad Q_s^2(r_2, b; Y) = \frac{r_2^2 e^{\bar{\alpha}_S \frac{\chi(\gamma_{cr})}{1-\gamma_{cr}} Y}}{\left(\vec{b} - \frac{1}{2}\vec{r}_2\right)^2 \left(\vec{b} + \frac{1}{2}\vec{r}_2\right)^2} \quad (2.14)$$

where (see Refs. [11, 36, 37])

$$\frac{\chi(\gamma_{cr})}{1-\gamma_{cr}} = -\frac{d\chi(\gamma_{cr})}{d\gamma_{cr}} \quad \text{where} \quad \chi(\gamma) = 2\psi(1) - \psi(\gamma) - \psi(1-\gamma) \leftarrow \text{kernel of the BFKL equation} \quad (2.15)$$

We denote below by  $\bar{\gamma} = 1 - \gamma_{cr}$  and will use Eq. (2.13) and Eq. (2.14) in the momentum transferred representation, viz.

$$N_{\mathcal{P}}(r_1, r_2; Y, Q_T) = \int d^2b e^{i\vec{Q}_T \cdot \vec{b}} N_{\mathcal{P}}(r_1, r_2; Y, b) \quad (2.16)$$

Integral of Eq. (2.16) with  $N_{\mathcal{P}}(r_1, r_2; Y, b)$  from Eq. (2.13) can be taken using the complex number description for the point on the plane (see Eq. (2.6) and Eq. (2.7)). The integral takes the form [10, 33]

$$N_{\mathcal{P}}(r_1, r_2; Y, Q_T) = (r_1^2 r_2^2)^{\bar{\gamma}} e^{\bar{\alpha}_S \chi(\gamma_{cr}) Y} \int d\rho_b e^{i\rho_Q^* \rho_b} \left( \frac{1}{\rho_b^2 - \rho_{12}^2} \right)^{\gamma} \int d\rho_b^* e^{i\rho_Q \rho_b^*} \left( \frac{1}{\rho_b^{*2} - \rho_{12}^{*2}} \right)^{\gamma} \quad (2.17)$$

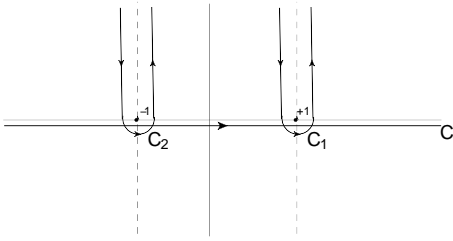


**Figure 3:** Contours of integration in Eq. (2.18).

Using new variables  $t = \rho_b/\rho_{12}$  and  $t^* = \rho_b^*/\rho_{12}$  and the integral representation of Hankel functions (see formulae **8.422(1,2)** in Ref. [34])

$$H_\nu^{(1,2)}(z) = \frac{\Gamma(\frac{1}{2} - \nu)}{\pi i \Gamma(\frac{1}{2})} \left( \frac{1}{2} z \right)^\nu \oint_{C_{1,2}} dt e^{izt} (t^2 - 1)^{\nu - \frac{1}{2}} \quad (2.18)$$

where contours  $C_1$  and  $C_2$  are shown in Fig. 3, we obtain that

$$N_{\mathcal{P}}(r_1, r_2; Y, Q_T) = C^2(\gamma) r_{12}^2 e^{\bar{\alpha}_S \chi(\gamma) Y} \left( \frac{r_1^2 r_2^2}{r_{12}^4} \right)^\gamma (Q^2 r_{12}^2)^{-\frac{1}{2} + \gamma} J_{\frac{1}{2} - \gamma}(\rho_Q^* \rho_{12}) J_{\frac{1}{2} - \gamma}(\rho_Q \rho_{12}^*) \quad (2.19)$$

where  $2J_\nu(z) = H^{(1)}(z) + H_\nu^{(2)}(z)$ ;  $\vec{r}_{12} = \frac{1}{2}(\vec{r}_1 - \vec{r}_2)$  and

$$C(\gamma) = 2^{-\frac{5}{2} + \gamma} \pi \frac{\Gamma(\frac{1}{2})}{\Gamma(\gamma)} \quad (2.20)$$

Two limits will be useful for further presentation:

$$N_{\mathcal{P}}(r_1, r_2; Y, Q_T) \xrightarrow{Q_T \rightarrow 0} C^2(\gamma) r_{12}^2 e^{\bar{\alpha}_S \chi(\gamma) Y} \left( \frac{r_1^2 r_2^2}{r_{12}^4} \right)^\gamma \quad (2.21)$$

$$\xrightarrow{Q_T^2 r_{12}^2 \gg 1} \frac{2}{\pi} C^2(\gamma) r_{12}^2 e^{\bar{\alpha}_S \chi(\gamma) Y} \left( \frac{r_1^2 r_2^2}{r_{12}^4} \right)^\gamma (Q^2 r_{12}^2)^{-1 + \gamma} \cos^2(\pi\gamma/2) e^{i\vec{Q} \cdot \vec{r}_{12}} \quad (2.22)$$

Eq. (2.21) can be re-written at  $r_1 \ll r_2$  in the form :

$$N_{\mathcal{P}}(r_1, r_2; Y, Q_T) \xrightarrow{Q_T \rightarrow 0, r_1 \ll r_2} C^2(\gamma) r_{12}^2 (r_1^2 Q_s^2(Y, r_2))^\gamma \quad \text{with } Q_s^2 = \frac{1}{r_2^2} e^{\bar{\alpha}_S \frac{\chi(\gamma)}{\gamma} Y};$$

$$\xrightarrow{Q_T r_2 \gg 1, r_1 \ll r_2} \frac{2}{\pi} C^2(\gamma) \cos^2(\pi\gamma/2) e^{i\vec{Q} \cdot \vec{r}_{12}} e^{\bar{\alpha}_S \chi(\gamma) Y} \frac{1}{Q_T^2} (Q_T^2 r_1^2)^\gamma \quad (2.23)$$

One can see that we can write a simple interpolation formula which we will bear in our mind in our estimates.

$$N_{\mathcal{P}}(r_1, r_2; Y, Q_T) = C^2(\gamma) r_{12}^2 (r_1^2 Q_s^2(Y, r_2))^\gamma (1 + a(\gamma) Q_T^2 r_{12}^2)^{-1 + \gamma} \quad \text{with } a^{-1 + \gamma}(\gamma) = \frac{2}{\pi} \cos^2(\pi\gamma/2) \quad (2.24)$$

For  $N_{\mathcal{P}}$  in the vicinity of the saturation scale  $\gamma = \bar{\gamma} = 1 - \gamma_{cr}$ .



## 2.2 Inclusive production in dipole-dipole scattering: the BFKL Pomeron contribution

In this subsection we calculate the cross section of the inclusive production of gluon jet with the transverse momentum  $p_\perp$  at rapidity  $Y_1$  in the collision of two dipoles with the sizes  $r_1$  and  $r_2$  at rapidity  $Y$  and at impact parameter  $b$ . The general formula which shows the  $k_T$ -factorization [40], has been derived in Ref. [41] and it takes the form

$$\frac{d\sigma}{d^2b dY_1 d^2p_\perp} = \frac{2C_F}{\alpha_s(2\pi)^4} \frac{1}{p_\perp^2} \int d^2\vec{B} d^2\vec{r}_\perp e^{i\vec{p}_\perp \cdot \vec{r}_\perp} \nabla_\perp^2 N^G(Y_1; r_\perp, r_1; b) \nabla_\perp^2 N^G(Y - Y_1; r_\perp, r_2; |\vec{b} - \vec{B}|) \quad (2.25)$$

where

$$N^G(Y; r_\perp, r_i; b) = 2N(Y; r_\perp, r_i; b) - N^2(Y; r_\perp, r_i; b), \quad (2.26)$$

Evaluating Eq. (2.1) we need to know such cross section only for the BFKL Pomeron exchange for which Eq. (2.26) reduces to the following equation

$$N_{\mathcal{P}}^G(Y; r_\perp, r_i; b) = 2N_{\mathcal{P}}(Y; r_\perp, r_i; b) \quad (2.27)$$

Plugging Eq. (2.27) in Eq. (2.25) we have

$$N_{\mathcal{P}}^{\text{incl}}(Y, r_1, r_2, b, p_\perp, Y_1) = \frac{8C_F}{\alpha_s(2\pi)^4} \frac{1}{p_\perp^2} \int d^2\vec{B} d^2\vec{r}_\perp e^{i\vec{p}_\perp \cdot \vec{r}_\perp} \nabla_\perp^2 N_{\mathcal{P}}(Y_1; r_\perp, r_1; B) \nabla_\perp^2 N_{\mathcal{P}}(Y - Y_1; r_\perp, r_2; |\vec{b} - \vec{B}|) \quad (2.28)$$

It is worthwhile mentioning that  $b$  is the difference of the impact parameters between scattering dipoles while  $B$  is the impact parameter of the produced gluon with respect to the dipole with size  $r_1$ .

In the vicinity of the saturation scale  $N_{\mathcal{P}}$  takes the form of Eq. (2.13) and  $\nabla_\perp^2 N_{\mathcal{P}}(Y_1; r_\perp, r_1; b)$  is equal to

$$\begin{aligned} \nabla_\perp^2 N_{\mathcal{P}}(Y_1; r_\perp, r_1; b) &= \quad (2.29) \\ &= \phi_0 \bar{\gamma}^2 \left( \frac{r_1^2 r_2^2}{(\vec{b} - \vec{r}_{12})^2 (\vec{b} + \vec{r}_{12})^2} e^{\bar{\alpha}_S \frac{\chi(\gamma_{cr})}{1-\gamma_{cr}} Y} \right)^{\bar{\gamma}} \left( \frac{2\vec{r}}{r^2} - \frac{\vec{b} - \vec{r}_{12}}{(\vec{b} - \vec{r}_{12})^2} + \frac{\vec{b} + \vec{r}_{12}}{(\vec{b} + \vec{r}_{12})^2} \right)^2 \end{aligned}$$

However, it turns out that it is more convenient to use  $\nabla_\perp^2 N_{\mathcal{P}}(Y_1; r_\perp, r_1; b)$  in momentum representation, namely,

$$\int d^2b e^{i\vec{Q}_T \cdot \vec{b}} \nabla_\perp^2 N_{\mathcal{P}}(Y_1; r_\perp, r_1; b) = \nabla_\perp^2 N_{\mathcal{P}}(Y_1; r_\perp, r_1; Q_T) \quad (2.30)$$

Using Eq. (2.19) for  $N_{\mathbb{P}}(Y_1; r_\perp, r_1; Q_T)$  and  $\nabla_r^2 = 4\partial_\rho\partial_{\rho^*}$  we obtain( denoting  $r_\perp \equiv r_0$ )

$$\begin{aligned} \nabla_\perp^2 N_{\mathbb{P}}(Y_1; r_\perp, r_1; Q_T) &= 4\phi_0 C^2(\gamma) r_{01}^2 e^{\bar{\alpha}_S \chi(\gamma) Y} \left( \frac{r_1^2 r_0^2}{r_{01}^4} \right)^\gamma (Q^2 r_{01}^2)^{-\frac{1}{2}+\gamma} \\ &\times \left\{ \left( \frac{\gamma}{\rho_r} - \frac{\frac{1}{2}+\gamma}{\rho_{01}} \right) J_{\frac{1}{2}-\gamma}(\rho_Q^* \rho_{01}) + \frac{1}{2} \rho_Q^* \left( J_{-\frac{1}{2}-\gamma}(\rho_Q^* \rho_{01}) - J_{-\frac{3}{2}-\gamma}(\rho_Q^* \rho_{01}) \right) \right\} \\ &\times \left\{ \left( \frac{\gamma}{\rho_r^*} - \frac{\frac{1}{2}+\gamma}{\rho_{01}^*} \right) J_{\frac{1}{2}-\gamma}(\rho_Q \rho_{01}^*) + \frac{1}{2} \rho_Q \left( J_{-\frac{1}{2}-\gamma}(\rho_Q \rho_{01}^*) - J_{-\frac{3}{2}-\gamma}(\rho_Q \rho_{01}^*) \right) \right\} \end{aligned} \quad (2.31)$$

We need to estimate

$$N_{\mathbb{P}}^{\text{incl}}(Y, r_1, r_2, Q_T, p_\perp, Y_1) = \int d^2 b e^{i\vec{Q}_T \cdot \vec{b}} N_{\mathbb{P}}^{\text{incl}}(Y, r_1, r_2, b, p_\perp, Y_1) \quad (2.32)$$

for calculation of the diagrams of Fig. 2. From Eq. (2.28) and Eq. (2.31) we obtain

$$\begin{aligned} N_{\mathbb{P}}^{\text{incl}}(Y, r_1, r_2, Q_T, p_\perp, Y_1) &= \\ &\frac{8 C_F}{\alpha_s (2\pi)^4} \frac{1}{p_\perp^2} \int d^2 \vec{r}_\perp e^{i\vec{p}_\perp \cdot \vec{r}_\perp} \nabla_\perp^2 N_{\mathbb{P}}(Y_1; r_\perp, r_1; Q_T) \nabla_\perp^2 N_{\mathbb{P}}(Y - Y_1; r_\perp, r_2; Q_T) \end{aligned} \quad (2.33)$$

For  $Q_T \rightarrow 0$  Eq. (2.32) reduces to the following equation (see Eq. (2.31))

$$\begin{aligned} N_{\mathbb{P}}^{\text{incl}}(Y, r_1, r_2, Q_T = 0, p_\perp, Y_1) &= \\ &= \frac{8 C_F}{\alpha_s (2\pi)^4} C^4(\bar{\gamma}) \bar{\gamma}^2 \frac{\phi_0^2}{p_\perp^2} \int \frac{d^2 r_\perp}{r_\perp^4} e^{i\vec{p}_\perp \cdot \vec{r}_\perp} r_1^2 r_2^2 \left( r^2 Q_s^2(r_1, Y - Y_1) \right)^{\bar{\gamma}} \left( r^2 Q_s^2(r_2, Y_1) \right)^{\bar{\gamma}} \\ &= \frac{8 C_F}{\alpha_s (2\pi)^4} \frac{\phi_0^2}{p_\perp^2} \int \frac{d^2 r_\perp}{r_\perp^4} e^{i\vec{p}_\perp \cdot \vec{r}_\perp} r_1^2 r_2^2 \left( r^2 Q_s^2(r_1, Y - Y_1) \right)^{\bar{\gamma}} \left( r^2 Q_s^2(r_2, Y_1) \right)^{\bar{\gamma}} \\ &= \bar{\phi}_0^2 \frac{8 C_F}{\alpha_s (2\pi)^4} 2^{-3+4\bar{\gamma}} r_1^2 r_2^2 \frac{\Gamma(1-2\bar{\gamma})}{\Gamma(2-2\bar{\gamma})} \left( \frac{Q_s^2(r_1, Y - Y_1)}{p_\perp^2} \right)^{\bar{\gamma}} \left( \frac{Q_s^2(r_2, Y_1)}{p_\perp^2} \right)^{\bar{\gamma}} \end{aligned} \quad (2.34)$$

$$\text{where } Q_s^2(r_1, Y - Y_1) = \frac{1}{r_1^2} \exp\left(\bar{\alpha}_S \frac{\chi(\gamma_{cr})}{1-\gamma_{cr}} (Y - Y_1)\right) \text{ and } Q_s^2(r_1, Y_1) = \frac{1}{r_2^2} \exp\left(\bar{\alpha}_S \frac{\chi(\gamma_{cr})}{1-\gamma_{cr}} Y_1\right)$$

### 2.3 Inclusive production in dipole-dipole scattering: non-linear equation

The main features of the inclusive production which we will use in our calculation of the first loop diagram, is the suppression of this production inside the saturation region. It follows directly from the general expression of Eq. (2.25) since  $N^G(Y_1; r_\perp, r_1; b) \xrightarrow{r_\perp^2 Q_s^2 \gg 1} 1$  while  $\nabla_\perp^2 N^G(Y_1; r_\perp, r_1; b) \xrightarrow{r_\perp^2 Q_s^2 \gg 1} 0$ . Honestly, these features do not appear in the simple diagram of Fig. 2, they manifest themselves only in the diagrams of Fig. 12 which describes the Pomeron loop in the dense environment. However, we believe that it is needed to discuss these features now since they are essential for our calculations.

In the saturation region the amplitude shows the geometric scaling behaviour [46] and the solution of the BFKL equation deeply inside of this region takes the following form [47]

$$N(z = \ln(r^2 Q_s^2)) = 1 - \exp\left(-\frac{z^2}{2\kappa}\right); \quad N^G(z = \ln(r^2 Q_s^2)) = 1 - \exp\left(-\frac{z^2}{\kappa}\right) \quad (2.35)$$

with  $\kappa = \frac{\chi(\gamma_{cr})}{1-\gamma_{cr}}$  and

$$-\nabla_{\perp}^2 N^G(z = \ln(r^2 Q_s^2)) = \frac{8(-\kappa + 2z^2)}{\kappa^2} \exp\left(-\frac{z^2}{\kappa}\right) \quad (2.36)$$

One can see that  $\nabla_{\perp}^2 N^G(z = \ln(r^2 Q_s^2))$  falls down and only  $z \approx 1$  is essential.

In the vicinity of the saturation scale  $N = 1 - \exp\left(-\phi_0(r^2 Q_s^2)^{1-\gamma_{cr}}\right)$  (see Ref. [47]) which leads to

$$\nabla_{\perp}^2 N^G\left(T = 2\phi_0(r^2 Q_s^2)^{1-\gamma_{cr}}\right) = (1 - \gamma_{cr})^2 \frac{4T}{r^2} \left(T - \frac{1}{2} \frac{1 - 2\gamma_{cr}}{1 - \gamma_{cr}}\right) e^{-T} \quad (2.37)$$

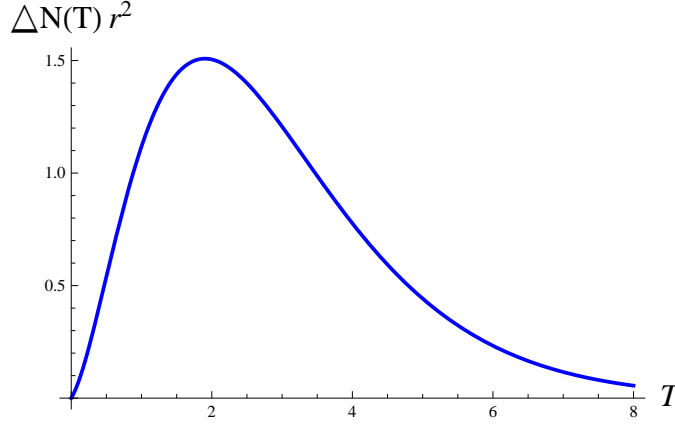


**Figure 4:**  $r^2 \nabla_{\perp}^2 N^G(T = 2\phi_0 r^2 Q_s^2)$  of Eq. (2.37) versus  $T$

One can see that  $\nabla^2 N^G$  has a maximum at  $T \sim 2$  and the integral over  $T$  is equal to  $8.39(1 - \gamma_{cr})^2 / r^2$ .

## 2.4 Rapidity correlations

In this section we calculate the rapidity correlations that stem from the diagram of Fig. 2. Eq. (2.13) in the momentum representation takes the form

$$\begin{aligned} \frac{d\sigma}{dY_1 dY_2 d^2 p_{\perp,1} d^2 p_{\perp,2}} &= \frac{4\pi^2 \bar{\alpha}_S^4}{N_c^2} \int_{Y_1}^Y dY' \int_{Y_0}^{Y_2} dY'' \quad (2.38) \\ &\int \frac{d^2 R_1}{R_1^4} \int \frac{d^2 R_2}{R_2^4} N_{\mathcal{P}}(Y - Y'; R_p, R_1, Q_T = 0) \int d^2 R'_1 \int d^2 R'_2 K(R_1, R'_1) \\ &\int d^2 Q_T N_{\mathcal{P}}^{\text{incl}}(Y' - Y'', R'_1, R'_2, Q_T | p_{\perp,1}, Y_1) N_{\mathcal{P}}^{\text{incl}}(Y' - Y'', \vec{R}_1 - \vec{R}'_1, \vec{R}_2 - \vec{R}'_2, Q_T | p_{\perp,2}, Y_2) \\ &K(R_2, R'_2) N_{\mathcal{P}}(Y'' - Y_0; R_2, R_A, Q_T = 0) \end{aligned}$$

Our main goal to find the largest contribution. As has been discussed in the previous section all Pomerons in the loop have the largest contributions in the vicinity of the saturation scale while the upper and low Pomerons can contribute inside of the saturation domain. Recall that for the Pomerons in the loop  $\gamma \rightarrow \bar{\gamma} = 1 - \gamma_{cr}$  in Eq. (2.19) - Eq. (2.24).

Let us concentrate our effort on  $Q_T$  integration considering three kinematic regions:

1.  $Q_T R_1 \ll 1$  and  $Q_T R_2 \ll 1$ . We will see below that both  $R'_1$  and  $|\vec{R}_1 - \vec{R}'_1|$  are of the order of  $R_1$  as well as  $R'_2$  and  $|\vec{R}_2 - \vec{R}'_2|$  are of the order of  $R_2$ . Using Eq. (2.21) one can see that  $\nabla_{\perp}^2 N_{\mathbb{P}}(Y - Y'; r_{\perp}, R_1; Q_T)$  as well as others  $\nabla_{\perp}^2 N_{\mathbb{P}}$  entering Eq. (2.32) and Eq. (2.38) do not depend on  $Q_T$ . Hence the integral over  $d^2 Q_T$  diverges in this region and the upper limit of integration gives the main contribution.
2.  $Q_T R_1 \sim 1$  and  $Q_T R_2 \ll 1$ . For hadron-nucleus collisions we expect that the main contributions would come from the saturation region in which  $R_2$  is proportional to  $1/Q_s(A; Y'')$  while  $R_1 \propto 1/Q_s(\text{proton}; Y - Y')$  and we expect that  $R_2 \ll R_1$  since  $Q_s(A; Y'') \gg Q_s(\text{proton}; Y - Y')$ . In this region  $\nabla_{\perp}^2 N_{\mathbb{P}}(Y_1 - Y''; r_{\perp}, R_2; Q_T)$  and  $\nabla_{\perp}^2 N_{\mathbb{P}}(Y_2 - Y''; r'_{\perp}, R_2; Q_T)$  do not depend on  $Q_T$  while  $\nabla_{\perp}^2 N_{\mathbb{P}}(Y' - Y_1; r_{\perp}, R_1; Q_T)$  and  $\nabla_{\perp}^2 N_{\mathbb{P}}(Y' - Y_2; r'_{\perp}, R_2; Q_T)$  are in the region of Eq. (2.22) and give contribution proportional to  $Q^{-2(1-\bar{\gamma})}$  each. Therefore, the integral has a form  $d^2 Q_T Q_T^{-4(1-\bar{\gamma})}$ . Recalling that  $\bar{\gamma} = 1 - \gamma_{cr} = 0.63$  one can see that the integral diverges in this region.
3.  $Q_T R_1 \gg 1$  and  $Q_T R_2 \gg 1$ . The integrant has the  $Q_T$  dependance which is  $(Q_T^2)^{-4(1-\bar{\gamma})}$  and the integral converges. Therefore the main contribution stems from the region when  $Q_T \propto 1/R_2$  and it is proportional to  $(R_2^2)^{3-4\bar{\gamma}}$ .
4.  $Q_T R_1 \gg 1$  and  $Q_T R_2 \gg 1$ . The integral over  $Q_T$  takes the form (assuming that  $r \ll R_1$  and/or  $R_2$ )

$$\begin{aligned} \int_{Q_T > 1/R_2} \frac{d^2 Q_T}{4\pi^2} (Q_T^2)^{-4(1-\bar{\gamma})} e^{2i\vec{Q}_T \cdot (\vec{R}_1 + \vec{R}_2)} &\rightarrow \frac{1}{4\pi^2} \int \frac{d^2 Q_T J_0(2Q_T |\vec{R}_1 + \vec{R}_2|)}{(Q_T^2 + 1/R_2^2)^{4(1-\bar{\gamma})}} = \\ &= \frac{1}{2\pi\Gamma(4-4\bar{\gamma})} (|\vec{R}_1 + \vec{R}_2| R_2)^{3-4\bar{\gamma}} K_{3-4\bar{\gamma}} \left( 2 \frac{|\vec{R}_1 + \vec{R}_2|}{R_2} \right) \end{aligned} \quad (2.39)$$

Concluding this discussion we see that the typical  $Q_T \approx 1/R_2^2$  where  $R_2$  is the size of the smallest dipole in triple Pomeron vertices. One can also see that Eq. (2.39) leads to  $|\vec{R}_1 + \vec{R}_2| \approx R_2$  or  $R_1 \rightarrow R_2$ . Based on these two features we can re-write Eq. (2.38) in the following way

$$\begin{aligned} \frac{d\sigma}{dY_1 dY_2 d^2 p_{\perp,1} d^2 p_{\perp,2}} &= \frac{4\pi^2 \bar{\alpha}_S^4}{N_c^2} \langle Q_T^2 \rangle \int_{Y_1}^Y dY' \int_{Y_0}^{Y_2} dY'' \int \frac{d^2 R_1}{R_1^4} \int \frac{d^2 R_2}{R_2^4} \\ N_{\mathbb{P}}(Y - Y'; R_p, R_1, Q_T = 0) &\int d^2 R'_1 \int d^2 R'_2 K(R_1, R'_1) N_{\mathbb{P}}^{\text{incl}}(Y' - Y'', R'_1, R'_2, Q_T = 0 | p_{\perp,1}, Y_1) \\ N_{\mathbb{P}}^{\text{incl}}(Y' - Y'', \vec{R}_1 - \vec{R}'_1, \vec{R}_2 - \vec{R}'_2, Q_T = 0 | p_{\perp,2}, Y_2) &K(R_2, R'_2) N_{\mathbb{P}}(Y'' - Y_0; R_2, R_A, Q_T = 0) \end{aligned} \quad (2.40)$$

where we estimate the value of  $\langle Q_T^2 \rangle$  using Eq. (2.24)

$$\begin{aligned} \langle Q_T^2 \rangle &= \frac{1}{2\pi} \int Q_T dQ_T \frac{J_0 \left( 2Q_T |\vec{R}_1 + \vec{R}_2| \right)}{\left( 1 + a(\bar{\gamma}) Q_T^2 R_2^2 \right)^{4(1-\bar{\gamma})}} \\ &= \frac{1}{2\pi\Gamma(4(1-\bar{\gamma}))} \frac{1}{a(\bar{\gamma}) R_2^2} \left( \frac{(\vec{R}_1 + \vec{R}_2)^2}{aR_2^2} \right)^{3/2-2\bar{\gamma}} K_{-3+4\bar{\gamma}} \left( 2 \frac{|\vec{R}_1 + \vec{R}_2|}{\sqrt{a(\bar{\gamma})} R_2} \right) \end{aligned} \quad (2.41)$$

Integrating over angle  $\varphi$  we obtain

$$\bar{Q}_T^2(\kappa) = \int d\varphi \langle Q_T^2 \rangle(\varphi, \kappa) \quad (2.42)$$

where  $\kappa = R_1/R_2$ . This function is shown in Fig. 5. One can see the steep decrease for  $\kappa > 1$  and, therefore, we can replace  $\langle Q_T^2 \rangle$  by

$$\langle\langle Q_T^2 \rangle\rangle = \int d\varphi d\kappa \langle Q_T^2 \rangle(\varphi, \kappa) = 0.0154 \delta(\kappa - 1) \quad (2.43)$$

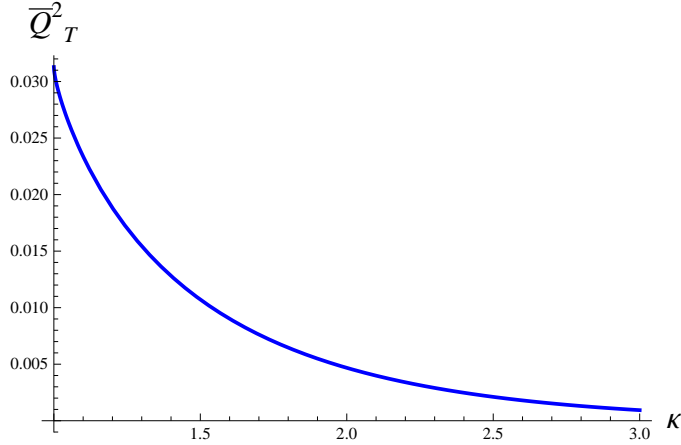


**Figure 5:**  $\bar{Q}_T^2(\kappa)$  defined in Eq. (2.42) versus  $\kappa = R_1/R_2$ .

Notice that each  $N_{IP}(Y_1; r_\perp, r_i; R_2)$  in Eq. (2.41) takes the form (see Eq. (2.9), Eq. (2.10) and Eq. (2.11))

$$N_{IP}(Y; r_\perp, r_i; R_2) = \int_{\epsilon-i\infty}^{\epsilon+i\infty} \frac{d\gamma}{2\pi i} \frac{(\gamma - \frac{1}{2})^2}{(\gamma(1-\gamma))} b_\gamma \left( \frac{r^2}{r_i^2} \right)^\gamma e^{\omega(\gamma)Y} \quad (2.44)$$

One can see that in Eq. (2.40) we have

$$\int d^2 R'_1 K(R_1, R'_1) \left( \frac{r^2}{R_1'^2} \right)^{\gamma_1} \left( \frac{r'^2}{|\vec{R}_1 - \vec{R}'_1|^2} \right)^{\gamma_2} = C_1(\gamma_1, \gamma_2) \left( \frac{r^2}{R_1^2} \right)^{\gamma_1} \left( \frac{r'^2}{R_1'^2} \right)^{\gamma_2} \quad (2.45)$$

where

$$C_1(\gamma_1, \gamma_2) = \pi \frac{B(-\gamma_1, -\gamma_2)}{(1 + \gamma_1 + \gamma_2) B(1 + \gamma_1, 1 + \gamma_2)} = \pi \frac{\Gamma(-\gamma_1) \Gamma(-\gamma_2) \Gamma(1 + \gamma_1 + \gamma_2)}{\Gamma(1 + \gamma_1) \Gamma(1 + \gamma_2) \Gamma(-\gamma_1 - \gamma_2)} \quad (2.46)$$

where  $B(x, y)$  is the Euler beta-function (see formula **8.38** of Ref. [34]). We introduce the Feynman parameters, using formula **3.198** of Ref. [34], to take the integral of Eq. (2.45).

The upper and lower Pomerons enter at  $Q_T = 0$  and both of them have the form the same as in Eq. (2.24). Plugging Eq. (2.24), Eq. (2.34), Eq. (2.43) and Eq. (2.46) in Eq. (2.40) we have the following expression

$$\frac{d\sigma}{dY_1 dY_2 d^2 p_{\perp,1} d^2 p_{\perp,2}} = 0.0154 \frac{4\pi^2 \bar{\alpha}_S^4}{N_c^2} \frac{8C_F}{\bar{\alpha}_S(2\pi)^4} \frac{1}{p_{\perp,1}^2} \frac{8C_F}{\bar{\alpha}_S(2\pi)^4} \frac{1}{p_{\perp,2}^2} \int \frac{\pi dr^2}{r^4} J_0(rp_{\perp,1}) \int \frac{\pi dr'^2}{r'^4} J_0(r'p_{\perp,2})$$

$$R_p^2 R_p^2 \mathcal{U}(\bar{\gamma}) \int_{r^2}^{R_p^2} dR_1^2 \delta\left(\frac{R_1}{R_2} - 1\right) \frac{dR_2^2}{R_2^2} \int_{Y_1}^Y dY' \int_{Y_0}^{Y_2} dY'' \Phi(r, r'; R_1, R_2, Y, Y', Y''; Y_1, Y_2) \quad (2.47)$$

$$\Phi(r, r'; R_1, R_2, Y, Y', Y''; Y_1, Y_2) = \left( T(R_1, R_p, Y - Y') T(R_2, R_p, Y'') T(r, R_1, Y' - Y_1) \right. \\ \left. \times T(r, R_2, Y_1 - Y'') T(r', R_1, Y' - Y_2) T(r', R_2, Y_2 - Y'') \right)^{\bar{\gamma}} \quad (2.48)$$

where

$$T(r_1, r_2; Y) = \frac{r_1^2}{r_2^2} \exp\left(\frac{\omega(\gamma_{cr})}{1 - \gamma_{cr}} Y\right) \quad \text{for } r_1 < r_2 \quad (2.49)$$

and

$$\mathcal{U}(\bar{\gamma}) = \bar{\phi}_0^4 \left( \frac{(\bar{\gamma} - \frac{1}{2})^2}{\bar{\gamma}(1 - \bar{\gamma})} b_{\bar{\gamma}} \right)^2 C^2(1 + \bar{\gamma}, 1 + \bar{\gamma}) \quad (2.50)$$

We can trust Eq. (2.47) only if all Pomerons approaching the saturation scale, i.e.

$$T(R_1, R_p, Y - Y') \rightarrow 1; \quad T(R_2, R_p, Y'') \rightarrow 1; \quad (2.51)$$

$$T(r, R_1, Y' - Y_1) \rightarrow 1; \quad T(r, R_2, Y_1 - Y'') \rightarrow 1; \quad (2.52)$$

$$T(r', R_1, Y' - Y_2) \rightarrow 1; \quad T(r', R_2, Y_2 - Y'') \rightarrow 1; \quad (2.53)$$

The maximal contribution to the diagram with the BFKL Pomerons which contributions can be trusted in perturbative QCD stem from the region where we have the sign of equality for all Pomerons, i.e. in the equations: Eq. (2.51), Eq. (2.52) and Eq. (2.53). For such kinematic region we calculate the diagram of Fig. 2 in the region where  $R_p^2 Q_s^2(p; Y) \approx 1$  as well as  $R_2^2 Q_s^2(A; Y'') \approx 1$  and  $R_1^2 Q_s^2(\text{proton}; Y - Y') \approx 1$ . We illustrate with Fig. 6 this region of integration drawing the first enhanced diagrams in the two dimensional plane  $(\ln(1/r^2), Y)$ .

However, as we will see below, we cannot keep all Pomerons in the vicinity of the saturation scale. On the other hand we have to keep all Pomerons in the Pomeron loop in the kinematic region close to

the saturation scale since, as we have discussed, only in this kinematic region the inclusive production gives the largest contributions. The best choice will be if the upper and low Pomerons will be inside the saturation domain where their amplitudes reach the unitarity limit  $N_{\mathbb{P}} \rightarrow 1$ . Finally, we are looking for the contribution in the following kinematic region:

$$T(R_1, R_p, Y - Y') \leq 1; \quad T(R_2, R_p, Y'') \leq 1; \quad (2.54)$$

$$T(r, R_1, Y' - Y_1) \approx 1; \quad T(r, R_2, Y_1 - Y'') \approx 1; \quad (2.55)$$

$$T(r', R_1, Y' - Y_2) \approx 1; \quad T(r', R_2, Y_2 - Y'') \approx 1; \quad (2.56)$$

Eq. (2.55) we can re-write in the following way:

$$\begin{aligned} T(R_1, R_p, Y - Y') &= \frac{1}{T(r, R_1, Y' - Y_1)} \frac{r^2}{R_p^2} e^{\frac{\omega(\gamma_{cr})}{1-\gamma_{cr}}(Y-Y_1)} = \frac{1}{T(r, R_1, Y' - Y_1)} r^2 Q_s^2(p, Y - Y_1); \\ T(R_2, R_p, Y'') &= \frac{1}{T(r, R_2, Y_1 - Y'')} \frac{r^2}{R_p^2} e^{\frac{\omega(\gamma_{cr})}{1-\gamma_{cr}}(Y_1)} = \frac{1}{T(r, R_2, Y_1 - Y'')} r^2 Q_s^2(p, Y_1); \end{aligned} \quad (2.57)$$

with

$$Q_s^2(p; Y) = \frac{1}{R_p^2} \exp\left(\bar{\alpha}_S \frac{\chi(\gamma_{cr})}{1-\gamma_{cr}} Y\right) \quad \text{and} \quad Q_s^2(A; Y) = \frac{A}{R_A^2} \exp\left(\bar{\alpha}_S \frac{\chi(\gamma_{cr})}{1-\gamma_{cr}} Y\right) \quad (2.58)$$

In Eq. (2.57) we introduce the saturation momentum for nucleus ( $Q_s(A; Y)$ ). Strictly speaking in the simple diagram, that we consider,  $N_{\mathbb{P}}^{\text{incl}}(Y_1, r; R_A)$  is proportional to  $AN_{\mathbb{P}}^{\text{incl}}(Y_1, r; R_p)$ . However, we will show in the next section that more complicated diagrams lead to  $N_{\mathbb{P}}^{\text{incl}}(Y_1, r; R_A) \propto (r^2 Q_s^2(A; Y_1 - 0))^{\bar{\gamma}}$ .

Taking into account Eq. (2.57) Eq. (2.48) can be re-written in the form

$$\begin{aligned} \Phi(r, r'; R_1, R_2, Y, Y', Y''; Y_1, Y_2) &= \\ &\left( r^2 Q_s^2(A, Y_1) r^2 Q_s^2(p, Y - Y_1) T(r', R_1, Y' - Y_2) T(r', R_2, Y_2 - Y'') \right)^{\bar{\gamma}} \end{aligned} \quad (2.59)$$

One can see that we can satisfy conditions of Eq. (2.56) only if

$$\frac{R_1^2}{R_2^2} = \exp\left(\frac{\omega(\gamma_{cr})}{1-\gamma_{cr}}(Y'' + Y' - 2Y_2)\right) \quad (2.60)$$

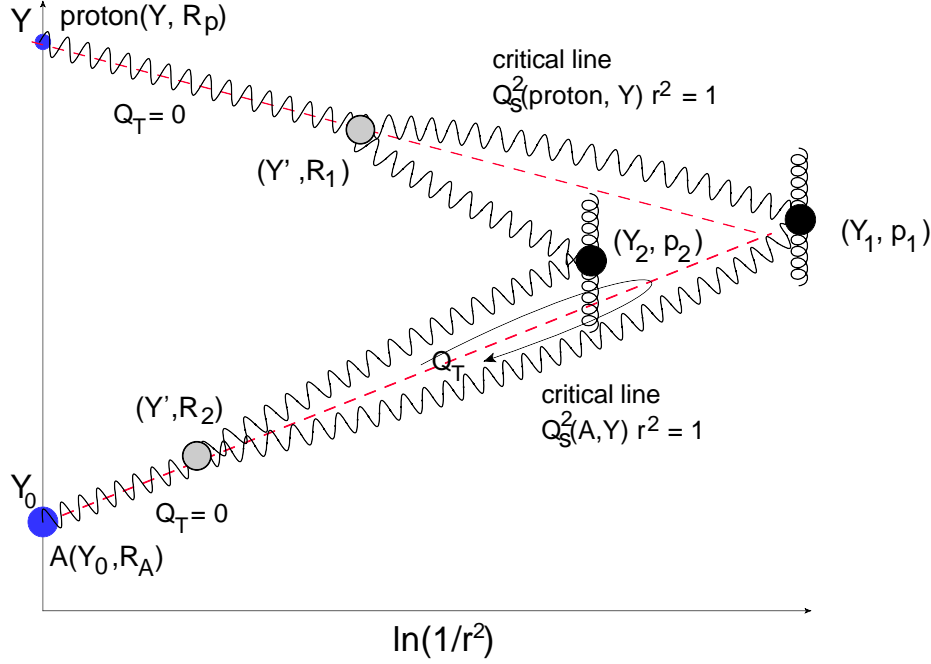


**Figure 6:** The first enhanced (loop) diagram for two particle correlation. Wavy lines denote the BFKL Pomerons. Helix lines show the gluons. Black blob stands for the Mueller vertex for inclusive production of gluon jet with the transverse momentum  $p_{\perp,1}$  ( $p_{\perp,2}$ ), respectively. Blue blobs describe the interaction of the BFKL Pomeron with the proton and the nucleus. Dashed red line corresponds to the critical line for proton-nucleus scattering.

Since this ratio is equal to 1, one sees that  $Y'' + Y' = 2Y_2$ . Finally

$$\int_{r^2}^{R_p^2} dR_1^2 \delta\left(\frac{R_1}{R_2} - 1\right) \frac{dR_2^2}{R_2^2} \int_{Y_1}^Y dY' \int_{Y_0}^{Y_2} dY'' \Phi(r, r'; R_1, R_2, Y, Y', Y''; Y_1, Y_2) = \quad (2.61)$$

$$\int_{r^2}^{R_p^2} dR_2^2 \int_{Y_1}^Y dY' \frac{1}{\omega(\gamma_{cr})} \left( r^2 Q_s^2(A, Y_1) r^2 Q_s^2(p, Y - Y_1) \frac{r'^4}{R_2^4} \exp\left(\bar{\alpha}_s \frac{\chi(\gamma_{cr})}{1 - \gamma_{cr}} (Y' - Y'')\right) \right)^{\bar{\gamma}} =$$

$$\int_{r^2}^{R_p^2} dR_2^2 \frac{1}{2\omega^2(\gamma_{cr})} \left\{ e^{2\omega(\gamma_{cr})(Y - Y_2)} - e^{2\omega(\gamma_{cr})(Y_1 - Y_2)} \right\} \left( r^2 Q_s^2(A, Y_1) r^2 Q_s^2(p, Y - Y_1) \frac{r'^4}{R_2^4} \right)^{\bar{\gamma}} =$$

$$\int_{r^2}^{R_p^2} dR_2^2 \frac{1}{2\omega^2(\gamma_{cr})} \left\{ \left( r^2 Q_s^2(A, Y_1) r^2 Q_s^2(p, Y - Y_1) r'^2 Q_s^2(R_2; Y - Y_2) r'^2 Q_s^2(R_2; Y_2 - Y'') \right)^{\bar{\gamma}} - \right.$$

$$\left. \left( r^2 Q_s^2(A, Y_1) r^2 Q_s^2(p, Y - Y_1) r'^2 Q_s^2(R_2; Y_1 - Y_2) r'^2 Q_s^2(R_2; Y_1 - Y_2) \right)^{\bar{\gamma}} \right\} \quad (2.62)$$

where  $Q_s(R_2; Y)$  is the saturation scale of Eq. (2.58) where  $R_p^2$  or  $R_A^2$  is replaced by  $R_2^2$ ,

The first term in Eq. (2.62) corresponds to  $Y' = Y$  and it is shown in Fig. 8-a for  $Y_1 = Y_2 = \frac{1}{2}Y$ ,



while the second term stems from  $Y' = Y_1$  (see Fig. 8-b).

One can see from Eq. (2.55) and Eq. (2.53) that we can have four BFKL Pomerons in the vicinity of the saturation region only for  $Y_1$  and  $Y_2$  that satisfy the equations:  $Q_s^2(p; Y - Y_1) = Q_s^2(A; Y_1)$  and  $Q_s^2(p; Y - Y_2) = Q_s^2(A; Y_2)$ . This region is shown in Fig. 8-a and we expect the largest contributions at  $p_{\perp,1}^2 \sim 1 / \left( R_p^2 \exp \left( \bar{\alpha}_S \frac{\chi(\bar{\gamma})}{\bar{\gamma}} (Y - Y_1) \right) \right)$  and  $p_{\perp,1}^2 \sim p_{\perp,2}^2 \exp \left( -\bar{\alpha}_S \frac{\chi(\bar{\gamma})}{\bar{\gamma}} (Y_1 - Y_2) \right)$ .

In the vicinity of the saturation scale  $N_{\mathbb{P}}$  takes the form<sup>§</sup> (see Refs. [17, 38, 39])

$$N_{\mathbb{P}}(r_1, r_2, Y, Q_T = 0; Y) = \phi_0 r_2^2 (r_1^2 Q_s^2(r_2, Y))^{\bar{\gamma}} \exp \left( - \frac{z^2}{2\omega''_{\gamma\gamma}(\gamma = \gamma_{cr}, 0) Y} \right) \quad (2.63)$$

where  $z = \ln \left( r_1^2 Q_s^2(r_2, Y) \right)$ .

We calculate the diagram of Fig. 8-a assuming Eq. (2.63) for  $N_{\mathbb{P}}$ . This assumption can be justified only in the limited kinematic region where  $\ln \left( Q_s^2(A; Y_1) / Q_s^2(p; Y - Y_1) \right) \ll \sqrt{2\pi\omega''_{\gamma\gamma}(\gamma = \gamma_{cr}, 0) Y_i}$  where  $Y_i$  is a minimum from  $Y - Y_1$  and  $Y_1$ .

Eq. (2.63) allows us to estimate the range in rapidities in which we can trust our evaluation of this diagram. As has been mention only at rapidity  $Y_1$  from the equation  $Q_s(p; Y - Y_1) = Q_s(A; Y_1)$  all four Pomerons in the loop can be considered in the saturation region, However, we really used the form of the amplitude from Eq. (2.63) but replacing  $\exp \left( - \frac{z^2}{2\omega''_{\gamma\gamma}(\gamma = \gamma_{cr}, 0) Y} \right)$  by unity. Rewriting this factor in terms of the saturation scale and deviation from it the factor for the Pomeron exchange with rapidity  $Y - Y_1$  in the loop takes the form

$$\exp \left( - \frac{z^2}{2\omega''_{\gamma\gamma}(\gamma = \gamma_{cr}, 0) Y} \right) = \exp \left( - \frac{\chi(\gamma_{cr})}{1 - \gamma_{cr}} \frac{\ln^2(r^2 Q_s^2(p, Y - Y_1))}{2\chi''_{\gamma\gamma}(\gamma = \gamma_{cr}, 0) \ln(Q_s^2(p, Y - Y_1) / Q_s^2(p, 0))} \right) \quad (2.64)$$

As has been discussed  $r^2 = 1 / Q_s^2(A, Y_1)$ , therefore, we can replace the Pomeron exchange by  $(r^2 Q_s^2(p, Y - Y_1))^{1 - \gamma_{cr}}$  if

$$e^{\Psi} = \exp \left( - \frac{\chi(\gamma_{cr})}{1 - \gamma_{cr}} \frac{\ln^2(Q_s^2(p, Y - Y_1) / Q_s^2(A; Y_1))}{2\chi''_{\gamma\gamma}(\gamma = \gamma_{cr}, 0) \ln(Q_s^2(p, Y - Y_1) / Q_s^2(p, 0))} \right) \rightarrow 1 \text{ or } \Psi \ll 1 \quad (2.65)$$

In Fig. 7 we plotted  $\Psi$  for the LHC energy  $W = 7TeV$  using the KLN parameterization for the saturation scale (see Ref. [50]). One can see that we can use our approach in the wide range of rapidities.

The last integration over  $R_2$  in Eq. (2.62) brings factor  $1 / (2\bar{\gamma} - 1)$  and two limits of integrations:  $R_2 = R_p$  and  $R_2 = r$  correspond to Fig. 8-a and Fig. 8-b, respectively,

Integrating over  $r$  and  $r'$  we obtain the following expression for the double inclusive cross section

$$\frac{d\sigma}{dY_1 dY_2 d^2 p_{\perp,1} d^2 p_{\perp,2}} = N_0^2 \phi_0^4, \frac{8 C_F}{\alpha_s(2\pi)^4} \frac{8 C_F}{\alpha_s(2\pi)^4} R_p^4 R_A^2 \quad (2.66)$$

$$\times \left( \frac{Q_s^2(p; Y - Y_1)}{p_{\perp,1}^2} \right)^{\bar{\gamma}} \left( \frac{Q_s^2(p; Y - Y_2)}{p_{\perp,2}^2} \right)^{\bar{\gamma}} \left( \frac{Q_s^2(A; Y_1 - Y_0)}{p_{\perp,1}^2} \right)^{\bar{\gamma}} \left( \frac{Q_s^2(A; Y - Y_2)}{p_{\perp,2}^2} \right)^{\bar{\gamma}}$$

<sup>§</sup>The expression for  $Q_s(Y)$  should be changed from  $\ln(Q_s^2(Y) / Q_s^2(Y = Y_0)) = \frac{\chi(\gamma_{cr})}{1 - \gamma_{cr}} (Y - Y_0)$  to more complicated expression (see Refs. [17, 36, 37]).

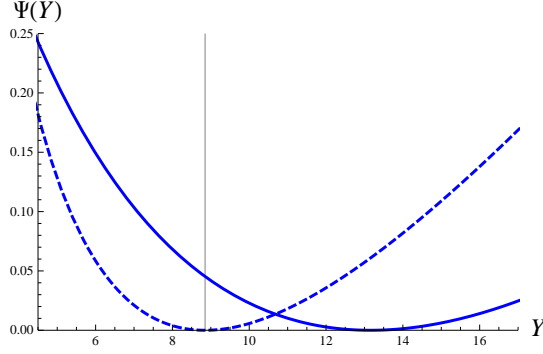


**Figure 7:** Function  $\Psi$  of Eq. (2.65) versus rapidity at  $W = 7TeV$ . The vertical line show the  $Y_1 = \frac{1}{2}Y$ . The solid line shows  $\Psi$  for proton-gold scattering while the dashed line corresponds to the proton-proton scattering.

where we assumed that all  $z_i \ll \sqrt{2\pi\omega''_{\gamma\gamma}(\gamma = \gamma_{cr}, 0) Y_i}$ . It should be stressed that Eq. (2.66) is valid for  $p_{i,\perp} \sim Q_s$ .

We introduce factor  $\phi_0$  (see Eq. (2.14)) which is the value of the  $N_P(r^2 Q_s^2)$  at  $r^2 Q_s^2 = 1$ . Generally speaking,  $N_0$  is the non-perturbative amplitude of Pomeron-nucleon scattering at low energy. We estimate the value of this amplitude by the contribution of the BFKL Pomeron in the saturation region replacing Green's functions for upper and low Pomerons in Fig. 2 by unity.

$$N_0^2 = n_d^2 0.0154 \frac{4\pi^3 \bar{\alpha}_S^4}{N_c^2} C^2 (1 + \bar{\gamma}, 1 + \bar{\gamma}) \frac{1}{4 (\bar{\alpha}_S \chi(\gamma_{cr}))^2} \quad (2.67)$$

where  $n_d$  is the number of the dipoles in the nucleon. In doing this estimates we assumed that the colorless dipoles are correct degrees of freedom for the non-perturbative QCD. For  $\bar{\alpha}_S = 0.2$   $N_0^2 = 1.53 n_d^2$ . We also included in  $N_0^2$  all  $\pi$ 's and numerical factors that stem from integrations over  $R_2, R_1$  and  $Y'$  in Eq. (2.61).

For hadron-hadron collisions  $R_A - R_p$  and integrating over  $p_{\perp,1}$  and  $p_{\perp,2}$  we see that  $p_{\perp,1}^2 \sim Q_s(p; Y_1 - Y_0)$  and  $p_{\perp,1}^2 \sim p_{\perp,2}^2 \exp\left(-\bar{\alpha}_S \frac{\chi(\bar{\gamma})}{\bar{\gamma}} (Y_1 - Y_2)\right)$  and using Eq. (2.66) we obtain

$$\int d^2 p_{\perp,1} d^2 p_{\perp,2} \frac{d\sigma}{dY_1 dY_2 d^2 p_{\perp,1} d^2 p_{\perp,2}} = \quad (2.68)$$

$$N_0^2 \phi_0^4 \frac{8 C_F}{\alpha_s (2\pi)^4} \frac{8 C_F}{\alpha_s (2\pi)^4} R_p^4 R_p^2 Q_s^2(p; Y_1) Q_s^2(p; Y_2) \left( \frac{Q_s^2(p; Y - Y_1)}{Q_s^2(p; Y_1)} \right)^{2\bar{\gamma}}$$

For the second term of  $\left\{ \dots \right\}$  in Eq. (2.61) the main contribution stems from  $R_2 = R_1 \rightarrow r \approx r'$  and the reduced diagram is shown in Fig. 8-b which describes the rapidity correlations inside one parton shower. Fig. 8-a gives the contribution in the restricted kinematic range of rapidities as has been discussed above. The largest contribution stems from the diagram of Fig. 9 in which the upper and lower Pomerons are in the saturation region. However, only two of four Pomerons in the loop can be near to the saturation momentum and this diagram is needed to be calculate using new vertices has been estimated in Ref. [42].

It means that this diagram has the same structure as shown in Fig. 8-b and can be calculated in framework of the BFKL Pomeron calculus only for  $Y_1 - Y_2 \gg 1$ . Therefore, we can neglect this contribution for the most interesting case of long range rapidity correlations.

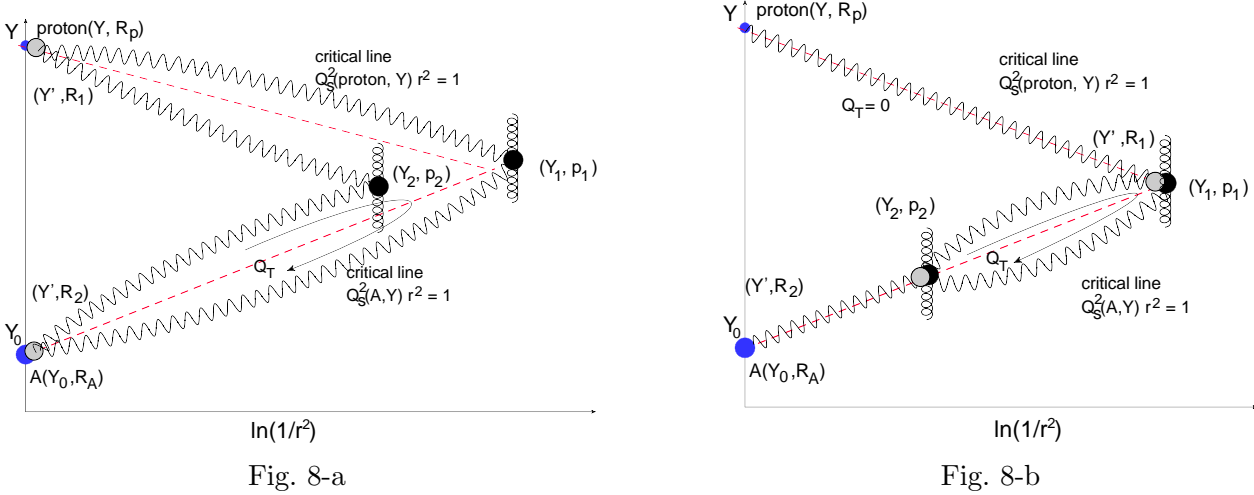


**Figure 8:** The first enhanced (loop) diagram for two particle correlation after integration over rapidities. Wavy lines denote the BFKL Pomerons. Helix lines show the gluons. Black blob stands for the Mueller vertex for inclusive production of gluon jet with the transverse momentum  $p_{\perp,1}$  ( $p_{\perp,2}$ ), respectively. Blue blobs describe the interaction of the BFKL Pomeron with the proton and the nucleus. Dashed red line corresponds to the critical line for proton-nucleus scattering.

The lesson we learned from our calculations, is that the integration over  $Y'$  and  $Y''$  reduces to  $Y' \rightarrow Y$  and  $Y'' \rightarrow 0$  in the Mueller enhanced diagram in the same way as for calculation of the total cross section (see Ref. [43]).

Using Eq. (2.68) and Eq. (2.34) we can estimate the rapidity correlation function, i.e.

$$R(Y_1, Y_2; Y) = \frac{\frac{1}{\sigma_{in}} \int \frac{d\sigma}{dY_1 dY_2 d^2 p_{\perp,1} d^2 p_{\perp,2}} dp_{\perp,1}^2 dp_{\perp,1}^2}{\frac{1}{\sigma_{in}} \int \frac{d\sigma}{dY_1 d^2 p_{\perp,1}} dp_{\perp,1}^2 \frac{1}{\sigma_{in}} \int \frac{d\sigma}{dY_2 d^2 p_{\perp,1}} dp_{\perp,1}^2} - 1 = \tilde{N}_0^2 I_Y(\bar{\gamma}) \frac{\sigma_{in}(Y)}{\pi R_p^2} - 1 \quad (2.69)$$

$$R(Y_1, p_{1,\perp}; Y_2, p_{2,\perp}; Y) = \frac{\frac{1}{\sigma_{in}} \int \frac{d\sigma}{dY_1 dY_2 d^2 p_{1,\perp} d^2 p_{2,\perp}}}{\frac{1}{\sigma_{in}} \int \frac{d\sigma}{dY_1 d^2 p_{\perp,1}} \frac{1}{\sigma_{in}} \int \frac{d\sigma}{dY_2 d^2 p_{\perp,1}}} - 1 = \tilde{N}_0^2 I_Y(\bar{\gamma}) \frac{\sigma_{in}(Y)}{\pi R_p^2} - 1 \quad (2.70)$$

where  $I_Y(\bar{\gamma})$  is the coefficient that will be written in Eq. (2.84) below.  $\tilde{N} = N/n_d$  and  $R$  is the size of the dipole inside of the hadron. We will discuss below both of these ingredients as well as the inelastic cross section  $\sigma_{in}(Y)$  in the next section.

## 2.5 Azimuthal angle correlations

As we have discussed in the introduction the azimuthal angle correlation arises from the terms  $(\vec{p}_{\perp,1} \cdot \vec{Q}_T)^2$  and  $(\vec{p}_{\perp,2} \cdot \vec{Q}_T)^2$  after integration over  $Q_T$  in the Pomeron loop in the diagram of Fig. 2 since

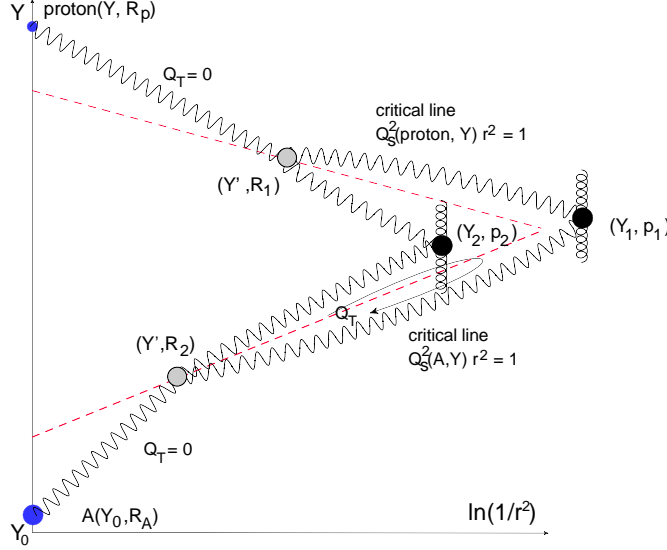


**Figure 9:** The first enhanced (loop) diagram for two particle correlation: the largest contribution in which the upper and lower Pomeron are in the saturation region. Wavy lines denote the BFKL Pomerons. Helix lines show the gluons. Black blob stands for the Mueller vertex for inclusive production of gluon jet with the transverse momentum  $p_{\perp,1}$  ( $p_{\perp,2}$ ), respectively. Blue blobs describe the interaction of the BFKL Pomeron with the proton and the nucleus. Dashed red line corresponds to the critical line for proton-nucleus scattering.

$\int d^2 Q_T (\vec{p}_{\perp,1} \cdot \vec{Q}_T)^2 (\vec{p}_{\perp,2} \cdot \vec{Q}_T)^2 \rightarrow (\vec{p}_{\perp,1} \cdot \vec{p}_{\perp,2})^2$ . Such terms in the coordinate representation that we are using here, stem from the terms  $(\vec{r}_{12} \cdot \vec{Q}_T)^2$  and  $(\vec{r}'_{12} \cdot \vec{Q}_T)^2$  in  $N_P(r_1, r_2, Y, Q_T)$  and  $N_P(r'_1, r'_2, Y, Q_T)$  (see Eq. (2.19)). These terms come from  $J_{\frac{1}{2}-\bar{\gamma}}(\rho_Q^* \rho_{12}) J_{\frac{1}{2}-\bar{\gamma}}(\rho_Q \rho_{12}^*)$ . For small  $Q_T$  we can see how these terms appear expanding  $J_{\frac{1}{2}-\bar{\gamma}}$ .

Indeed,

$$\begin{aligned}
& J_{\frac{1}{2}-\bar{\gamma}}(\rho_Q^* \rho_{12}) J_{\frac{1}{2}-\bar{\gamma}}(\rho_Q \rho_{12}^*) = \tag{2.71} \\
& = \left( \frac{1}{2^{\frac{1}{2}-\bar{\gamma}} \Gamma(\frac{3}{2}-\bar{\gamma})} \right)^2 \left\{ 1 + \frac{1}{2(-3+2\bar{\gamma})} Q_T^2 r_{12}^2 e^{2i(\phi-\psi)} \right\} \left\{ 1 + \frac{1}{2(-3+2\bar{\gamma})} Q_T^2 r_{12}^2 e^{-2i(\phi-\psi)} \right\} \\
& \rightarrow \left( \frac{1}{2^{\frac{1}{2}-\bar{\gamma}} \Gamma(\frac{3}{2}-\bar{\gamma})} \right)^2 \left\{ 1 + \frac{1}{(-3+2\bar{\gamma})} Q_T^2 r_{12}^2 \cos(2(\phi-\psi)) + \left( \frac{1}{2(-3+2\bar{\gamma})} \right)^2 Q_T^4 r_{12}^4 \right\} \\
& \rightarrow \left( \frac{1}{2^{\frac{1}{2}-\bar{\gamma}} \Gamma(\frac{3}{2}-\bar{\gamma})} \right)^2 \left\{ 1 + \frac{1}{(-3+2\bar{\gamma})} \left( 2 (\vec{Q}_T \cdot \vec{r}_{12})^2 - Q_T^2 r_{12}^2 \right) + \left( \frac{1}{2(-3+2\bar{\gamma})} \right)^2 Q_T^4 r_{12}^4 \right\}
\end{aligned}$$

In Eq. (2.71) we use the representation of complex numbers in the polar coordinates, for example,  $\rho_Q = Q e^{i\phi}$  and  $\rho_Q^* = Q e^{-i\phi}$ . The same type of contributions come from Eq. (2.31).

For  $Q_T r_{12} \gg 1$  we can see the same features since

$$\begin{aligned}
N_{\mathcal{P}}(r_1, r_2; Y, Q_T) &\xrightarrow{Q_T^2 r_{12}^2 \gg 1} \\
&\phi_0 C^2(\bar{\gamma}) \frac{2}{\pi} r_{12}^2 e^{\bar{\alpha}_S \chi(\gamma_{cr}) Y} \left( \frac{r_1^2 r_2^2}{r_{12}^4} \right)^{\bar{\gamma}} (Q_T^2 r_{12}^2)^{-1+\bar{\gamma}} \cos^2(\pi\bar{\gamma}/2) e^{i\vec{Q}_T \cdot \vec{r}_{12}} \\
&\left\{ (1/8)(\bar{\gamma}(\bar{\gamma}-2)(1-\bar{\gamma}^2)) + Q_T^2 r_{12}^2 e^{i2(\phi-\psi)} \right\} \left\{ (1/8)(\bar{\gamma}(\bar{\gamma}-2)(1-\bar{\gamma}^2)) + Q_T^2 r_{12}^2 e^{-i2(\phi-\psi)} \right\} / Q_T^4 r_{12}^4 \\
&= \phi_0 C^2(\bar{\gamma}) \frac{2}{\pi} r_{12}^2 e^{\bar{\alpha}_S \chi(\gamma_{cr}) Y} \left( \frac{r_1^2 r_2^2}{r_{12}^4} \right)^{\bar{\gamma}} (Q_T^2 r_{12}^2)^{-3+\bar{\gamma}} \cos^2(\pi\bar{\gamma}/2) e^{i\vec{Q}_T \cdot \vec{r}_{12}} \\
&\left\{ \left[ (1/8)(\bar{\gamma}(\bar{\gamma}-2)(1-\bar{\gamma}^2)) \right]^2 + (1/4)(\bar{\gamma}(\bar{\gamma}-2)(1-\bar{\gamma}^2)) \left( 2 \left( \vec{Q}_T \cdot \vec{r}_{12} \right)^2 - Q_T^2 r_{12}^2 \right) + Q_T^4 r_{12}^4 \right\}
\end{aligned} \tag{2.72}$$

However the largest contribution stems at  $r \ll R_1$  and  $r \ll R_2$  from Eq. (2.31) which can be re-written as

$$\begin{aligned}
\nabla_{\perp}^2 N_{\mathcal{P}}(Y_1; r_{\perp}, r_1; Q_T) &\rightarrow \\
&4 \phi_0 C^2(\bar{\gamma}) r_{01}^2 e^{\bar{\alpha}_S \chi(\gamma_{cr}) Y} \left( \frac{r_0^2 r_1^2}{r_{01}^4} \right)^{\bar{\gamma}} (Q^2 r_{01}^2)^{-\frac{1}{2}+\bar{\gamma}} \frac{\bar{\gamma}^2}{r^2} J_{\frac{1}{2}-\bar{\gamma}}(\rho_Q^* \rho_{01}) J_{\frac{1}{2}-\bar{\gamma}}(\rho_Q \rho_{01}^*)
\end{aligned} \tag{2.73}$$

where  $r_0 \equiv r_{\perp}$ .

Notice, that at  $Q_T \rightarrow 0$  Eq. (2.73) reduces to

$$\begin{aligned}
\nabla_{\perp}^2 N_{\mathcal{P}}(Y_1; r_{\perp}, r_1; Q_T) &\rightarrow \\
&4 \phi_0 C^2(\bar{\gamma}) r_{01}^2 e^{\bar{\alpha}_S \chi(\gamma_{cr}) Y} \left( \frac{r_0^2 r_1^2}{r_{01}^4} \right)^{\bar{\gamma}} \left( \frac{2^{-\frac{1}{2}\bar{\gamma}}}{\Gamma(3/2-\bar{\gamma})} \right)^2 \frac{\bar{\gamma}^2}{r^2} \left\{ 1 - \frac{1}{2(3-2\bar{\gamma})} (\rho_Q^2 \rho_{01}^{*2} + \rho_Q^* \rho_{01}^2) \right\} \\
&= 4 \phi_0 C^2(\bar{\gamma}) r_{01}^2 e^{\bar{\alpha}_S \chi(\gamma_{cr}) Y} \left( \frac{r_0^2 r_1^2}{r_{01}^4} \right)^{\bar{\gamma}} \left( \frac{2^{-\frac{1}{2}\bar{\gamma}}}{\Gamma(3/2-\bar{\gamma})} \right)^2 \frac{\bar{\gamma}^2}{r^2} \left\{ 1 - \frac{1}{(3-2\bar{\gamma})} \left( \vec{Q}_T \vec{r}_{01} \right)^2 \right\} \\
&= 4 \phi_0 C^2(\bar{\gamma}) r_{01}^2 e^{\bar{\alpha}_S \chi(\gamma_{cr}) Y} \left( \frac{r_0^2 r_1^2}{r_{01}^4} \right)^{\bar{\gamma}} \left( \frac{2^{-\frac{1}{2}\bar{\gamma}}}{\Gamma(3/2-\bar{\gamma})} \right)^2 \frac{\bar{\gamma}^2}{r^2} \left\{ 1 - \frac{1}{(3-2\bar{\gamma})} \left( \vec{Q}_T \vec{r} \right)^2 \right\}
\end{aligned} \tag{2.74}$$

We need to re-visit the integration over  $Q_T$  in Eq. (2.38) and re-analyzed this integration based on Eq. (2.71)-Eq. (2.74). Let us consider the integration over  $Q_T$  in three kinematic regions assuming that  $R_1 > R_2$ :

1.  $Q_T R_1 \ll 1$  and  $Q_T R_2 \ll 1$ . In this kinematic region all Pomerons in the loop enter at small arguments and they do not depend on  $Q_T$ . However, the azimuthal angle correlations stems from Eq. (2.74) leading to the additional factor which is proportional to  $\left( \vec{Q}_T \cdot \vec{r} \right)^2 \left( \vec{Q}_T \cdot \vec{r}' \right)^2$ . Therefore, the integration in this region leads to  $Q_T \rightarrow 1/R_1$ .

2.  $Q_T R_1 \sim 1$  and  $Q_T R_2 \ll 1$ . As has been discussed (see Eq. (2.38)) in this region  $\nabla_{\perp}^2 N_{\mathcal{P}}(Y_1 - Y''; r_{\perp}, R_2; Q_T)$  and  $\nabla_{\perp}^2 N_{\mathcal{P}}(Y_2 - Y''; r'_{\perp}, R_2; Q_T)$  do not depend on  $Q_T$  while  $\nabla_{\perp}^2 N_{\mathcal{P}}(Y' - Y_1; r_{\perp}, R_1; Q_T)$  and  $\nabla_{\perp}^2 N_{\mathcal{P}}(Y' - Y_2; r'_{\perp}, R_2; Q_T)$  are in the region of Eq. (2.22) and give contribution proportional to  $Q^{-2(1-\bar{\gamma})}$  each. However, for the analysis of the integration over  $Q_T$  we need to consider separately two sources of the angular correlations.

**2.1** The angle correlations comes from the Pomerons with the arguments  $Q_T R_1 \leq 1$ . In this case they stem from the contributions of Eq. (2.74) leading to the  $Q_T$  dependence of the following type:

$$\int d^2 Q_T \left( \vec{Q}_T \cdot \vec{r} \right)^2 \left( \vec{Q}_T \cdot \vec{r}' \right)^2 \frac{1}{(Q_T^2)^{2(1-\bar{\gamma}_{cr})}} \rightarrow (Q_T^2, \max)^{3+2\gamma_{cr}} = \left( \frac{1}{R_2^2} \right)^{3+2\gamma_{cr}} \quad (2.75)$$

**2.2** The angle correlations comes from the Pomerons with the arguments  $Q_T R_2 > 1$ . The source of the angular correlations is shown in Eq. (2.72). One can see that this equation generates the contribution which is proportional to  $(Q_T^2 R_2^2)^{-2(1-\bar{\gamma})} \left( \vec{Q}_T \cdot \vec{r} \right)^2 \left( \vec{Q}_T \cdot \vec{r}' \right)^2 / (Q_T^2 R_2^2)^4$  which leads to the convergent integral over  $Q_T$ .

3.  $Q_T R_1 \gg 1$  and  $Q_T R_2 \gg 1$ . The integrant has the  $Q_T$  dependance which is  $(Q_T^2)^{-4(1-\bar{\gamma})}$  which is multiplied by the factor:  $\left( \vec{Q}_T \cdot \vec{r} \right)^2 \left( \vec{Q}_T \cdot \vec{r}' \right)^2 / (Q_T^2 R_i^2)^4$ . Therefore, the integral converges.

Concluding this discussion we see that the most contribution in the integral over  $Q_T$  comes from the region **2.1** and the typical  $Q_T \approx 1/R_2^2$  assuming that  $R_2 < R_1$ . In other words, the typical values of the impact parameters in the Pomeron loops turns out to be about  $|\vec{b}_1 - \vec{b}_2| \sim R_2$  as in the case of rapidity correlations (see Eq. (2.38) and Eq. (2.39)). One can see that  $R_1 \rightarrow R_2$  from Eq. (2.39). In Fig. 10 we plot the integrant  $\Phi(Q_T)$  defined as

$$\frac{d\sigma}{dY_1 dY_2 d^2 p_{\perp,1} d^2 p_{\perp,2}} \propto \int d^2 Q_T \Phi(Q_T; R_1, R_2, r, r') \quad (2.76)$$

One can see that this function has a sharp maximum at  $Q_T \approx 1/R^2$ .

Our integral over  $Q_T$  in the diagram of Fig. 6 differs from the same integral in the case of rapidity correlations and it takes the following form for  $Q_T R_2 \gg 1$

$$I_{i,j,k,l}(r, r', R_1, R_2) = \int d^2 Q_T \left\{ Q_{T,i} Q_{T,j} Q_{T,k} Q_{T,l} \right\} (Q_T^2)^{4(1-\bar{\gamma})} \exp \left( i \vec{Q}_T \cdot \{ \vec{r}_{01} + \vec{r}_{02} + \vec{r}'_{01} + \vec{r}'_{02} \} \right) \Phi(r, r'; R_1, R_2, Y, Y', Y''; Y_1, Y_2) \quad (2.77)$$

where  $\vec{r}_{01} = \frac{1}{2}(\vec{r} + \vec{R}_1)$  and  $\vec{r}_{02} = \frac{1}{2}(\vec{r} + \vec{R}_2)$  while  $\vec{r}'_{01} = \frac{1}{2}(\vec{r}' + \vec{R}_1)$  and  $\vec{r}'_{02} = \frac{1}{2}(\vec{r}' + \vec{R}_2)$  and  $i, j, k, l$  are equal to 1 and 2.  $\Phi(r, r'; R_1, R_2, Y, Y', Y''; Y_1, Y_2)$  is the function given by Eq. (2.47).

This integral can be re-written in the form ( for brevity, we will use notation  $\Phi(r, r'; R_1, R_2)$  instead of  $\Phi(r, r'; R_1, R_2, Y, Y', Y''; Y_1, Y_2)$ ).

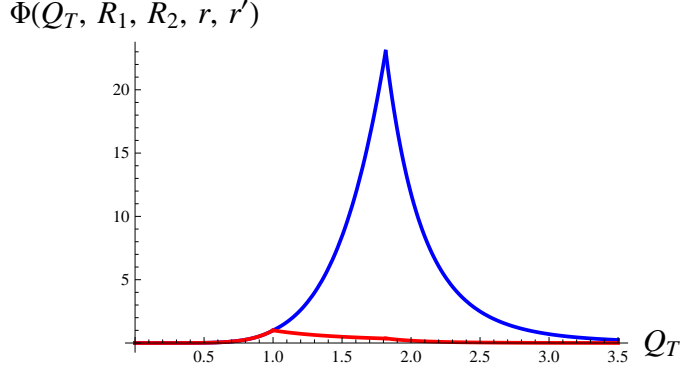


**Figure 10:** The integrand  $\Phi(Q_T; R_1, R_2, r, r')$  (see Eq. (2.76)) versus  $Q_T$ . The blue curve shows the contribution of the kinematical region 2.1 while the red one corresponds to the kinematic region 2.2. In the picture the values of  $R_1$  and  $R_2$  are chosen:  $R_1^2 = 1 \text{ GeV}^{-2}$  and  $R_2^2 = 0.3 \text{ GeV}^{-2}$ .

$$\begin{aligned}
I_{i,j,k,l}(r, r', R_1, R_2) &= \tag{2.78} \\
&= \int d^2 Q_T (Q_T^2)^{4(1-\bar{\gamma})} \left( \left\{ \nabla_{r_{01},i} \nabla_{r_{02},j} \nabla_{r'_{01},k} \nabla_{r'_{02},l} \right\} \exp \left( i \vec{Q}_T \cdot \{ \vec{r}'_{01} + \vec{r}'_{02} + \vec{r}'_{01} + \vec{r}'_{02} \} \right) \right) \Phi(r, r', R_1, R_2) = \\
&= (-1)^4 \int d^2 Q_T (Q_T^2)^{4(1-\bar{\gamma})} \exp \left( i \vec{Q}_T \cdot \{ \vec{r}'_{01} + \vec{r}'_{02} + \vec{r}'_{01} + \vec{r}'_{02} \} \right) \left( \left\{ \nabla_{r_{01},i} \nabla_{r_{02},j} \nabla_{r'_{01},k} \nabla_{r'_{02},l} \right\} \Phi(r, r', R_1, R_2) \right)
\end{aligned}$$

where function  $\Phi$  is the same as in Eq. (2.47). It should be noted that the second equation in Eq. (2.78) is derived using the integration by parts and taking into account that  $\Phi(r, r', R_1, R_2) \Big|_{r(r') \rightarrow -\infty}^{r(r') \rightarrow +\infty} = 0$ .

Considering  $r$  and  $r'$  being small ( $\ll R_1, R_2$ ) we restrict ourselves by the contribution given by Eq. (2.73). Eq. (2.78) can be re-written taking gradients in the form

$$I_{i,j,k,l}(r, r', R_1, R_2) = \int d^2 Q_T \left( \frac{1}{Q_T^2} \right)^{4(1-\bar{\gamma})} \exp \left( i \vec{Q}_T \cdot \{ \vec{r}'_{01} + \vec{r}'_{02} + \vec{r}'_{01} + \vec{r}'_{02} \} \right) \frac{R_{1,i} R_{1,k}}{R_1^4} \frac{R_{2,j} R_{2,l}}{R_2^4} \Phi(r, r', R_1, R_2) \tag{2.79}$$

Finally, the contribution to the double inclusive production takes the form

$$\begin{aligned}
\frac{d\sigma}{dY_1 dY_2 d^2 p_{\perp,1} d^2 p_{\perp,2}} &\propto \frac{4\pi^2 \bar{\alpha}_S^4}{N_c^2} \frac{8 C_F}{\alpha_s (2\pi)^4} \frac{1}{p_{\perp,1}^2} \frac{8 C_F}{\alpha_s (2\pi)^4} \frac{1}{p_{\perp,2}^2} \frac{(\vec{p}_{\perp,1} \cdot \vec{p}_{\perp,2})^2}{p_{\perp,1}^2 p_{\perp,2}^2} \\
&\times \int \frac{r dr}{r^2} \left( J_0(p_{\perp,1} r) - J_2(p_{\perp,1} r) \right) \int \frac{r' dr'}{r'^2} \left( J_0(p_{\perp,2} r') - J_2(p_{\perp,2} r') \right) \tag{2.80} \\
&R_p^2 R_p^2 \bar{U}(\bar{\gamma}) \int_{r^2}^{R_p^2} dR_1^2 \delta \left( \frac{R_1}{R_2} - 1 \right) \frac{dR_2^2}{R_2^2} \int_{Y_1}^Y dY' \int_{Y_0}^{Y_2} dY'' \frac{1}{4} \frac{1}{R_1^2} \frac{1}{R_2^2} \Phi(r, r'; R_1, R_2, Y, Y', Y''; Y_1, Y_2)
\end{aligned}$$

The difference between Eq. (2.80) and the calculations of rapidity correlation that has been done in the previous subsection is in the different factor  $\bar{U}(\bar{\gamma})$  and in the extra factors  $\frac{1}{4} \frac{1}{R_1^2} \frac{1}{R_2^2}$ . However these factors do not change qualitatively the character of integration over  $R_1$  and  $R_2$ : the integration over  $Q_T$  leads to  $R_1 = R_2 = R$  and to  $Q_T \approx 1/R$ . Therefore, we obtain that

$$\frac{1}{4} \frac{1}{R_1^2} \frac{1}{R_2^2} \longrightarrow 0.53 \frac{1}{4} \frac{1}{R^4} \quad (2.81)$$

where the numerical factor 0.53 reflect the difference in the averaging given by Eq. (2.43).

Eq. (2.81) can be translated into the following expression for  $\frac{d\sigma}{dY_1 dY_2 d^2 p_{\perp,1} d^2 p_{\perp,2}}$ :

$$\begin{aligned} \frac{d\sigma}{dY_1 dY_2 d^2 p_{\perp,1} d^2 p_{\perp,2}} &= I(\bar{\gamma}) N_0^2 \phi_0^4 \frac{8 C_F}{\alpha_s (2\pi)^4} \frac{8 C_F}{\alpha_s (2\pi)^4} \frac{(\vec{p}_{\perp,1} \cdot \vec{p}_{\perp,2})^2}{p_{\perp,1}^2 p_{\perp,2}^2} R_p^2 \frac{1}{p_{\perp,1}^2 p_{\perp,2}^2} \\ &\times \left( \frac{Q_s^2(Y - Y_1)}{p_{\perp,1}^2} \right)^{\bar{\gamma}} \left( \frac{Q_s^2(Y_2 - Y_0)}{p_{\perp,2}^2} \right)^{\bar{\gamma}} \left( \frac{Q_s^2(Y_1 - Y_0)}{p_{\perp,1}^2} \right)^{\bar{\gamma}} \left( \frac{Q_s^2(Y - Y_2)}{p_{\perp,2}^2} \right)^{\bar{\gamma}} \end{aligned}$$

In Eq. (2.82) factor  $I(\bar{\gamma})$  includes all numerical factors that depend on  $\gamma_{cr}$ .

Eq. (2.82) is written in the kinematic region where all factors  $Q_s^2/p_{\perp,i}^2 \leq 1$ . Integrating over  $p_{\perp,1}$  and  $p_{\perp,2}$  in this kinematic region we obtain for  $Y_1 < \frac{1}{2}(Y + Y_0)$  and  $Y_2 < \frac{1}{2}(Y + Y_0)$  that Eq. (2.82) takes the form

$$\begin{aligned} \int \frac{d\sigma}{dY_1 dY_2 d^2 p_{\perp,1} d^2 p_{\perp,2}} dp_{\perp,1}^2 dp_{\perp,1}^2 &= \quad (2.82) \\ \cos^2 \varphi I(\bar{\gamma}) N_0^2 \phi_0^4 \frac{8 C_F}{\alpha_s (2\pi)^4} \frac{8 C_F}{\alpha_s (2\pi)^4} R_p^2 &\left( \frac{Q_s^2(Y_1 - Y_0)}{Q_s^2(Y - Y_1)} \right)^{\bar{\gamma}} \left( \frac{Q_s^2(Y_2 - Y_0)}{Q_s^2(Y - Y_2)} \right)^{\bar{\gamma}} \end{aligned}$$

where  $\varphi$  is the azimuthal angle between vectors  $\vec{p}_{\perp,1}$  and  $\vec{p}_{\perp,2}$ . For the angular correlation function in proton-proton scattering we obtain

$$R(\cos \phi) = \frac{\frac{1}{\sigma_{in}} \int \frac{d\sigma}{dY_1 dY_2 d^2 p_{\perp,1} d^2 p_{\perp,2}} dp_{\perp,1}^2 dp_{\perp,1}^2}{\frac{1}{\sigma_{in}} \int \frac{d\sigma}{dY_1 d^2 p_{\perp,1}} dp_{\perp,1}^2 \frac{1}{\sigma_{in}} \int \frac{d\sigma}{dY_2 d^2 p_{\perp,1}} dp_{\perp,1}^2} - 1 = \cos^2 \phi I(\bar{\gamma}) \tilde{N}_0^2 \frac{\sigma_{in}(Y)}{R_p^2} \frac{1}{R_p^2 Q_s^2(Y_1) R_p^2 Q_s^2(Y_2)} \quad (2.83)$$

where  $\tilde{N}_0 = N_0^2/n_d^2$  and

$$I(\bar{\gamma}) = I_Y(\bar{\gamma}) \frac{\bar{\gamma}}{2(3-2\bar{\gamma})} = 0.53 \frac{1}{2\bar{\gamma}-1} \frac{1}{4} \left( \frac{1}{(3-2\bar{\gamma})} \right)^2 \frac{4}{\pi^2} \left( \frac{2^{-\frac{1}{2}+\bar{\gamma}}}{\Gamma(3/2-\bar{\gamma})} \right)^{-2} \approx 0.068 \quad (2.84)$$

In Eq. (2.84) we include factors from Eq. (2.50) and Eq. (2.74). Comparing this factor with the rapidity correlation we see that the azimuthal angle correlations are suppressed by factor  $0.63/(2(3-2\bar{\gamma}))^2 \approx 0.05$ . In addition we consider  $Y_1 > Y - Y_1$  and  $Y_2 > Y - Y_2$ .  $R_p = R$  is the size of the typical dipole inside of the hadron. One can see that the coefficient in front of  $\cos^2 \varphi$  is rather small in the angular correlation function mostly due to the large large multiplicity of the inclusively produced gluons which is proportional



to  $Q_s$ . It worthwhile mentioning that such suppression we did not see in the rapidity correlation function (see Eq. (2.69)). This suppression can be easily understood. Indeed, the angular correlations appear due to factor  $(\vec{r} \cdot \vec{Q}_T)^2 (\vec{r}' \cdot \vec{Q}_T)^2$  which has the value of the order  $(\langle Q_T^2 \rangle / p_{1,\perp}^2) (\langle Q_T^2 \rangle / p_{2,\perp}^2)$ . As has been shown the average  $Q_T$  turns out to be of the order of  $Q_T \sim 1/R$  where  $R$  is the size of the dipole in a hadron, while  $p_\perp \sim Q_s$ . Therefore, we expect that the angle correlations are suppressed as  $1/(R^2 Q_s^2)^2$ , as we saw in Eq. (2.83).

The coefficient in front of  $\cos^2 \varphi$  is not suppressed showing the possibility to find another definition of the correlation function with enhanced contribution of the angular correlations.

It is interesting to note that the correlations at fixed  $p_{\perp,1} \sim Q_s$  and  $p_{\perp,2} \sim Q_s$  take the following form

$$R(\cos \varphi, p_{\perp,1}, p_{\perp,2}) = \sigma_{in} \frac{\frac{d\sigma}{dY_1 dY_2 d^2 p_{\perp,1} d^2 p_{\perp,2}}}{\frac{d\sigma}{dY_1 d^2 p_{\perp,1}} \frac{d\sigma}{dY_2 d^2 p_{\perp,2}}} = \cos^2 \varphi I(\tilde{\gamma}) \tilde{N}_0^2 \frac{\sigma_{in}(Y)}{\pi R^2} \frac{1}{R_p^2 p_{1,\perp}^2 R_p^2 p_{2,\perp}^2} \quad (2.85)$$

$\sigma_{in}$  is the inelastic cross section for dipole-dipole scattering. From Fig. 11 we see that  $n_d$ 's ( the vertices of proton-BFKL Pomeron) cancel in the ratio of Eq. (2.83). We need the phenomenological approach for the soft high energy scattering based on CGC/saturation approach ( see Ref. [49] for first try to estimate  $\sigma_{in}$  in dipole-dipole scattering using a minimal phenomenological input). In numerical evaluations we use , in spirit of our approach to  $N_0$  ( see Eq. (2.67)),  $\sigma_{in} = \sigma_{in}(\text{proton-proton})/9$  assuming that we have 3 dipoles in a proton. For estimates, we consider  $\sigma_{in} = \sigma_{tot} - \sigma_{el} - \sigma_{diff}$ . The size of the dipole inside of the proton we chose to be equal  $R^2 \approx 1 \text{ GeV}^{-2}$ ( see Ref. [49]).

Substituting these values we obtain  $R(\cos \phi) \approx (0.48 / (R_p^2 Q_s^2(Y_1) R_p^2 Q_s^2(Y_2))) \cos^2 \varphi$  at the LHC energy  $W = 7 \text{ GeV}$  in the central region of rapidity  $Y_1 = Y_2 = Y/2$ . The large coefficient in front of  $\cos^2 \varphi$  indicates the enhanced diagrams can give a large contribution to the angular correlations. However, it should be noted that the accuracy of our estimates are rather low due to uncertainty in both the value of  $R$  and the number of dipoles in the proton.

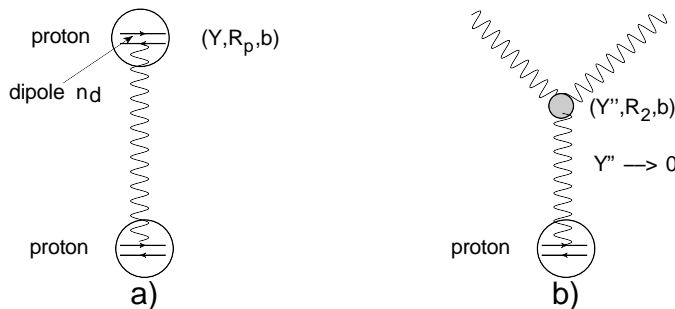


**Figure 11:**  $\sigma_{in}$  (see Fig. 11-a) and  $\tilde{N}_0$  (see Fig. 11-b) in Eq. (2.83).

We integrate Eq. (2.34) over  $p_\perp$  for calculating the single inclusive cross sections in the dominator of Eq. (2.83).

### 3. The first enhanced diagram in the saturation environment

In proton-nucleus scattering the simplest diagram of Fig. 2 cannot be considered as a good approximation for  $p_{\perp} \rightarrow Q_s$  since the Pomerons interact with the dense target (with nucleus). In Fig. 12 we demonstrate several examples of such interactions. Such interaction leads to the saturation of the parton (gluon) density [11–13] and in this section we wish to discuss the BFKL Pomeron Green’s function in the kinematic region when the Pomeron interaction with nucleus become essential.

#### 3.1 Equation for Pomeron Green’s function

For dilute-dense parton systems scattering the main contribution stem from ‘fan’ diagrams [11, 35] (see Fig. 12). In the case of the lower Pomeron in the first enhanced diagram (see Fig. 2 and Fig. 12) the sum of ‘fan’ diagrams leads to Balitsky-Kovchegov (BK) equation [15] (see Fig. 13), which takes the form

$$\begin{aligned} \frac{\partial N_{\mathbb{P}} \left( Y'' - Y_0; R_2, R_A, \vec{b}_2 \right)}{\partial Y''} &= \bar{\alpha}_S \int d^2 R'_2 K \left( R_2 | R'_2 \right) \left\{ N_{\mathbb{P}} \left( Y'' - Y_0; R'_2, R_A, \vec{b}_2 - \frac{1}{2}(\vec{R}_2 - \vec{R}'_2) \right) \right. \\ &+ N_{\mathbb{P}} \left( Y'' - Y_0; |\vec{R}_2 - \vec{R}'_2|, R_A, \vec{b}_2 - \frac{1}{2}\vec{R}'_2 \right) - N_{\mathbb{P}} \left( Y'' - Y_0; R_2, R_A, \vec{b}_2 \right) \\ &\left. - N_{\mathbb{P}} \left( Y'' - Y_0; R'_2, R_A, \vec{b}_2 - \frac{1}{2}(\vec{R}_2 - \vec{R}'_2) \right) N_{\mathbb{P}} \left( Y'' - Y_0; |\vec{R}_2 - \vec{R}'_2|, R_A, \vec{b}_2 - \frac{1}{2}\vec{R}'_2 \right) \right\} \end{aligned} \quad (3.1)$$

where the vertex  $K \left( R_2 | R'_2 \right)$  describes the decay of the dipole with the size  $R_2$  to two dipoles with sizes:  $R'_2$  and  $|\vec{R}_2 - \vec{R}'_2|$  and it is given by Eq. (2.2).

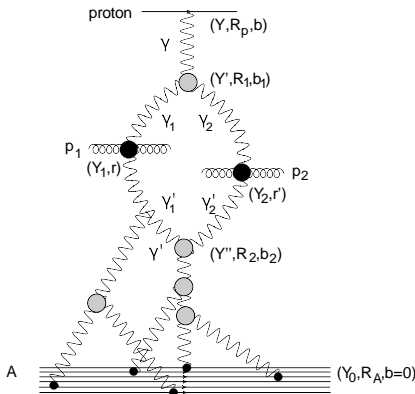


**Figure 12:** The interactions with the nucleus of a nucleus in the first enhanced diagram. Wavy lines denote the BFKL Pomerons. Helix lines show the gluons. Black blob stands for the Mueller vertex for inclusive production of gluon jet with the transverse momentum  $p_{\perp,1}$  ( $p_{\perp,2}$ ), respectively.

However BK equation is not enough since we need to find Green’s function of the BFKL Pomeron that propagates from coordinate  $(Y'', R_2)$  to coordinate  $(Y_1, r)$  and/or  $(Y_2, r')$  and interacts with the nucleus. This interactions are carried by the ‘fan’ diagrams as one can see in Fig. 14. The equation for Green’s

function takes the form (see the graphic representation in Fig. 14):

$$G(Y, r, b; Y', r'; b') = G^{\text{BFKL}}(Y - Y', r; r'; \vec{b} - \vec{b}') - \int_{Y'}^Y dY'' \iint d^2 r'' d^2 b'' G^{\text{BFKL}}(Y - Y'', r; r''; \vec{b} - \vec{b}'') \times K(r'', \hat{r}) G\left(Y'', \hat{r}, \vec{b}'' - \frac{1}{2}(\vec{r}'' - \hat{r}), Y', r', b'\right) N_{\mathcal{P}}\left(Y'', \vec{r}'' - \hat{r}; R_A; \vec{b}'' - \frac{1}{2}\hat{r}\right) \quad (3.2)$$

From Fig. 14 one can see that we can write the second equation for Green's function summing the diagrams as an evolution in  $Y'$ . The equation is

$$G(Y, r, b; Y', r'; b') = G^{\text{BFKL}}(Y - Y', r; r'; \vec{b} - \vec{b}') - \int_{Y'}^Y dY'' \iint d^2 r'' d^2 b'' G(Y, r, b; Y'', r'', b'') \times K(r'', \hat{r}) G^{\text{BFKL}}\left(Y'' - Y', \hat{r}, r'; \vec{b}'' - \vec{b}' - \frac{1}{2}(\vec{r}'' - \hat{r})\right) N_{\mathcal{P}}\left(Y'', \vec{r}'' - \hat{r}; R_A; \vec{b}'' - \frac{1}{2}\hat{r}\right) \quad (3.3)$$

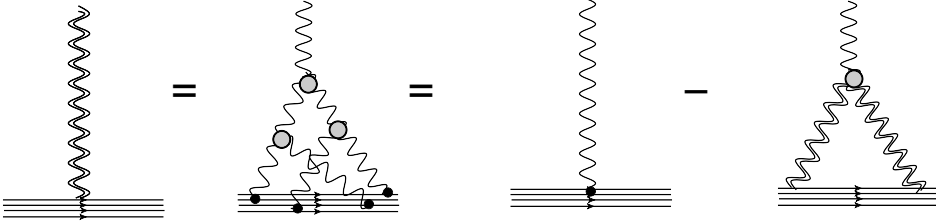


**Figure 13:** The graphic form of Balitsky-Kovchegov equation: fan diagrams. The double wavy lines denote the resulting Green's function of the BFKL Pomeron. Wavy lines denote the BFKL Pomeron. The gray circles show the triple Pomeron vertices.

Eq. (3.2) can be re-written in the differential form

$$\frac{\partial G(Y, r, b; Y', r'; b')}{\partial Y} = \bar{\alpha}_S \int d^2 r'' K(r|r'') \left\{ G\left(Y, r'', \vec{b} - \frac{1}{2}(\vec{r} - \vec{r}''); Y', r', b'\right) + G\left(Y, \vec{r} - \vec{r}'', \vec{b} - \frac{1}{2}\vec{r}'; Y', r', b'\right) - G(Y, r, b; Y', r', b') - G\left(Y, r'', \vec{b} - \frac{1}{2}(\vec{r} - \vec{r}''), Y', r', b'\right) N_{\mathcal{P}}\left(Y, \vec{r} - \vec{r}''; R_A; \vec{b} - \frac{1}{2}\vec{r}'\right) \right\} \quad (3.4)$$

while Eq. (3.3) takes the form

$$\begin{aligned} \frac{\partial G(Y, r, b; Y', r', b')}{\partial Y'} &= -\bar{\alpha}_S \int d^2 r'' K(r''|r') \left\{ G\left(Y, r, b; Y', r''; \vec{b}' - \frac{1}{2}(\vec{r}' - \vec{r}'')\right) \right. \\ &+ G\left(Y, r, b; Y', \vec{r}' - \vec{r}'', \vec{b}' - \frac{1}{2}\vec{r}'\right) - G(Y, r, b; Y', r', b') \\ &\left. - G\left(Y, r, b; Y', r''; \vec{b} - \frac{1}{2}(\vec{r}' - \vec{r}'')\right) N_{\mathbb{P}}\left(Y', \vec{r}' - \vec{r}''; R_A; \vec{b} - \frac{1}{2}\vec{r}'\right) \right\} \end{aligned} \quad (3.5)$$

Introducing  $\bar{G}(Y, r, b; Y', r', b') = r'^4 \bar{G}(Y, r, b; Y', r', b')$  we can re-write Eq. (3.5) as follows<sup>¶</sup>

$$\begin{aligned} \frac{\partial \bar{G}(Y, r, b; Y', r', b')}{\partial Y'} &= -\bar{\alpha}_S \int d^2 r'' K(r''|r') \left\{ \bar{G}\left(Y, r, b; Y', r''; \vec{b}' - \frac{1}{2}(\vec{r}' - \vec{r}'')\right) \right. \\ &+ \bar{G}\left(Y, r, b; Y', \vec{r}' - \vec{r}'', \vec{b}' - \frac{1}{2}\vec{r}'\right) - \bar{G}(Y, r, b; Y', r', b') \\ &\left. - \bar{G}\left(Y, r, b; Y', r''; \vec{b} - \frac{1}{2}(\vec{r}' - \vec{r}'')\right) N_{\mathbb{P}}\left(Y', \vec{r}' - \vec{r}''; R_A; \vec{b} - \frac{1}{2}\vec{r}'\right) \right\} \end{aligned} \quad (3.6)$$

One can see from Eq. (3.4) and Eq. (3.6) that  $G(r, Y, b; r', Y', b')$  can be factorized as

$$G(r, Y, b; r', Y', b') = G(r, Y, b) G(r', Y', b') \quad (3.7)$$

## 3.2 Solutions

### 3.2.1 The toy model

It is instructive to start the search for the solution to Eq. (3.4) in the simple toy-model [14, 44] in which all dipoles are assumed to have the same size. In this model the BFKL equation looks as follows

$$\frac{dN_{\mathbb{P}}^{\text{BFKL}}(Y, Y')}{dY} = \Delta_{\mathbb{P}} N_{\mathbb{P}}^{\text{BFKL}}(Y, Y') \quad \text{with solution} \quad N_{\mathbb{P}}^{\text{BFKL}}(Y - Y') = N_0 e^{\Delta_{\mathbb{P}}(Y - Y')} \quad (3.8)$$

where  $N_0$  is the value of the amplitude at  $Y = Y'$ . Note, that Green's function of the BFKL Pomeron in this model is equal to  $G_{\mathbb{P}}^{\text{BFKL}}(Y, Y') = \exp(\Delta_{\mathbb{P}}(Y - Y'))$ .

The BK equation takes the form

$$\frac{dN_{\mathbb{P}}^{\text{BK}}(Y, Y_0)}{dY} = \Delta_{\mathbb{P}} \left\{ N_{\mathbb{P}}^{\text{BK}}(Y, Y_0) - (N_{\mathbb{P}}^{\text{BK}}(Y, Y_0))^2 \right\} \quad (3.9)$$

Solution to this equation can be found and it looks as follows

$$N_{\mathbb{P}}^{\text{BK}}(Y, Y_0) = \frac{N_0}{N_0 + (1 - N_0) \exp(-\Delta_{\mathbb{P}}(Y - Y_0))} \quad (3.10)$$

---

<sup>¶</sup>We will use below for function  $\bar{G}$  notation  $G$  and , hope, it will not cause any misunderstanding.

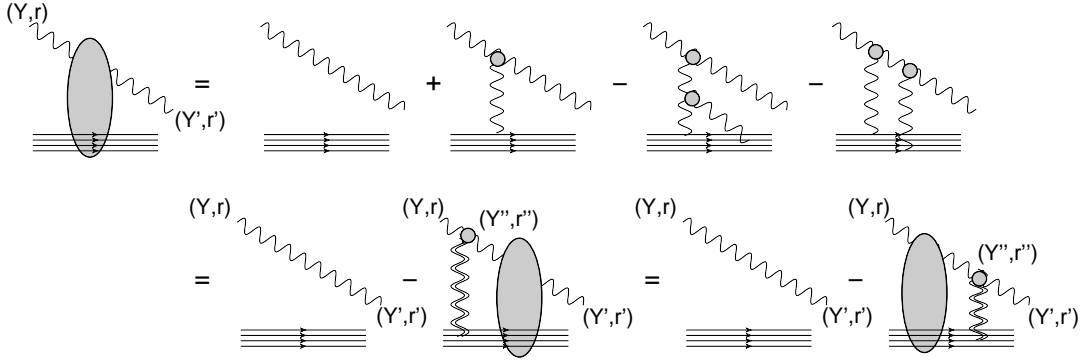


**Figure 14:** Equation for Green's function of the resulting BFKL Pomeron. The double wavy lines denote Green's function from the BK equation ( see Fig. 13). Wavy lines denote the BFKL Pomeron. The gray circles show the triple Pomeron vertices. The gray blobs describe the resulting Green's function.

where  $N_0$  is the value of the amplitude at  $Y = Y_0$ . One can see that  $N_P \rightarrow 1$  at  $Y \gg 1$  reproducing the saturation in this model.

Eq. (3.4) can be re-written in the following form

$$\frac{dG(Y, Y')}{dY} = \Delta_P \left\{ G(Y, Y') - G(Y, Y') N_P^{\text{BK}}(Y, Y_0) \right\} \quad (3.11)$$

It has solution in the form

$$G(Y, Y') = e^{\Delta_P(Y-Y')} \frac{N_0 e^{\Delta Y'} + 1 - N_0}{N_0 e^{\Delta Y} + 1 - N_0} = \frac{N_P^{\text{BK}}(Y, Y_0)}{N_P^{\text{BK}}(Y', Y_0)} \quad (3.12)$$

First, at small  $Y$  and  $Y'$  when both  $N_0 e^{\Delta Y'} \ll 1$  and  $N_0 e^{\Delta Y} \ll 1$  Eq. (3.12) reduces to the Green function of the BFKL Pomeron in this model  $G^{\text{BFKL}}(Y, Y') = \exp(\Delta_P(Y - Y'))$ . Second, at  $Y \gg 1$  and  $Y' \gg 1$   $G(Y, Y')$  is saturated reaching unity. Third, at  $Y' = 0$   $N_0 G(Y, 0) = N_P^{\text{BK}}(Y, 0)$  as it should be from the diagrams of Fig. 14.

### 3.2.2 Equations in the momentum representation

Eq. (3.4) and Eq. (3.5) look simpler in the momentum representation defined as

$$G(Y, r, b; Y', r', b') = r^2 r'^2 \int \frac{d^2 k}{(2\pi)^2} \frac{d^2 k'}{(2\pi)^2} G(Y, k, b; Y', k', b') \quad (3.13)$$

Considering  $b \gg r$  and  $b' \gg r'$  one can see that Eq. (3.4) and Eq. (3.5) take the forms

$$\frac{\partial G(Y, k, b; Y', k', b')}{\partial Y} = \quad (3.14)$$

$$\bar{\alpha}_S \left\{ \int d^2 k'' K^{BFKL}(k, k'') G(Y, k'', b; Y', k', b') - G(Y, k, b; Y', k', b') N(Y, k, b) \right\};$$

$$\frac{\partial G(Y, k, b; Y', k', b')}{\partial Y'} = \quad (3.15)$$

$$- \bar{\alpha}_S \left\{ \int d^2 k'' K^{BFKL}(k'', k') G(Y, k, b; Y', k'', b') - G(Y, k, b; Y', k', b') N(Y', k', b') \right\};$$

where the BFKL kernel  $K^{BFKL}(k, k'')$  takes the form [9, 17]

$$K^{BFKL}(k, k'') = \frac{1}{(\vec{k} - \vec{k}'')^2} - \frac{1}{2} \int \frac{k^2 d^2 k''}{k''^2 (\vec{k} - \vec{k}'')^2} \delta^{(2)}(\vec{k} - \vec{k}') \quad (3.16)$$

The graphical form of these equations is the same as for Eq. (3.4) and Eq. (3.5) in Fig. 14 where we need to replace  $r \rightarrow k$  and  $r' \rightarrow k'$ . It should be stressed that for large  $b$  and  $b' = b'$  since the BFKL kernel does not change the impact parameters of the dipoles.

In Fig. 15 we show the graphical form of the equation for Green's function  $G(Y, k, b; Y', k', b')$  in a different form:

$$\frac{\partial N(Y, k, b)}{\partial Y} = \int d^2 k' G(Y, k, b; Y', k', b) N(Y', k', b) \quad (3.17)$$

In derivation of Eq. (3.17) we use the following property of Green's function of the BFKL Pomeron which follows directly from t-channel unitarity [11, 48]:

$$G^{BFKL}(Y, k, b; Y', k', b) = \int d^2 k'' G^{BFKL}(Y, k, b; Y'', k'', b) G^{BFKL}(Y'', k'', b; Y', k', b) \quad (3.18)$$

All these equations should be solved with the following initial and boundary conditions which follow directly from Fig. 14 and Fig. 15, i.e.

$$G(Y, k, b; Y', k', b) \xrightarrow{Y' \rightarrow Y} G^{BFKL}(Y, k, b; Y' \rightarrow Y, k', b) = \delta^{(2)}(\vec{k} - \vec{k}');$$

$$\int d^2 k' G(Y, k, b; Y' = 0, k', b) N(Y' = 0, k', b) = N(Y, k, b) \quad (3.19)$$

where the second equation follows from Eq. (3.17).

### 3.2.3 Solution to the equations

We suggest the following ansatz for the solution

$$G(Y, k, b; Y', k', b) = \frac{N(Y, k, b)}{N(Y', k', b)} \delta^{(2)}(\vec{k} - \vec{k}'); \quad (3.20)$$

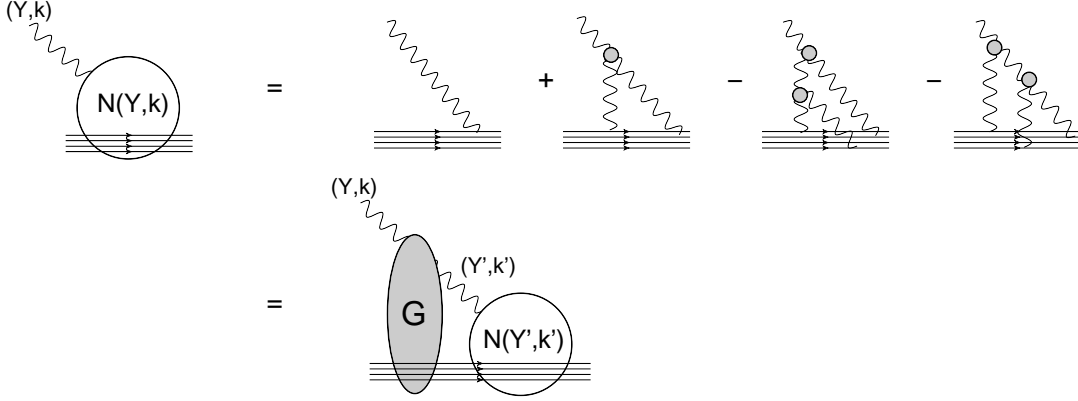


**Figure 15:** Equation for Green's function of the resulting BFKL Pomeron. Wavy lines denote the BFKL Pomerons. The gray circles show the triple Pomeron vertices. The gray blobs describe the resulting Green's function:  $G(Y, k, b; Y', k', b')$ . The white blobs denote Green's function from the BK equation (see Fig. 13).

This ansatz is motivated by the solution for the toy model (see Eq. (3.12)) and satisfies the boundary and initial conditions of Eq. (3.19). Now let us check that Eq. (3.14) and Eq. (3.15) are satisfied with this ansatz.

Substituting Eq. (3.20) in Eq. (3.14) we see that this equation reduces to

$$\begin{aligned} \frac{1}{N(Y', k', b)} \frac{\partial N(Y, k, b)}{\partial Y} \delta^{(2)}(\vec{k} - \vec{k}') &= \\ &= \bar{\alpha}_S \frac{1}{N(Y', k', b)} \left\{ K^{BFKL}(k, k') N(Y, k') - N^2(Y, k, b) \delta^{(2)}(\vec{k} - \vec{k}') \right\} \end{aligned} \quad (3.21)$$

Multiplying both parts of the equation by  $N(Y', k', b)$  and integrating over  $k'$  one can see that Eq. (3.21) takes the form

$$\frac{\partial N(Y, k, b)}{\partial Y} = \bar{\alpha}_S \left\{ \int d^2 k' K^{BFKL}(k, k') N(Y, k') - N^2(Y, k, b) \right\} \quad (3.22)$$

which is the Balitsky-Kovchegov equation for  $N$ .

Plugging Eq. (3.20) in Eq. (3.15) leads to the following expression

$$\begin{aligned} \frac{N(Y, k, b)}{N^2(Y', k', b)} \frac{\partial N(Y', k', b)}{\partial Y'} \delta^{(2)}(\vec{k} - \vec{k}') &= \\ &= \bar{\alpha}_S \frac{N(Y, k, b)}{N^2(Y', k', b)} \left\{ K^{BFKL}(k, k') N(Y, k') - N^2(Y', k') \delta^{(2)}(\vec{k} - \vec{k}') \right\} \end{aligned} \quad (3.23)$$

Multiplying by  $N^2(Y', k', b) / N(Y, k, b)$  we obtain the Balitsky-Kovchegov equation for  $N(Y', k', b)$ .

It is easy to check that the ansatz of Eq. (3.20) satisfies Eq. (3.17). Therefore, we can state that Eq. (3.20) is the solution to Eq. (3.14) and Eq. (3.15).

### 3.2.4 Solution to the equation in the vicinity of the saturation scale

Eq. (3.20) gives the general solution but, as we have discussed, for the evaluation of the correlation function Green's function of the BFKL Pomeron is actually needed only in the vicinity of the saturation scale (see Fig. 2 and Fig. 12). In the vicinity of the saturation scale we can neglect the non-linear terms in Eq. (3.4) and Eq. (3.5) and the solution to the linear equation takes the form of Eq. (2.63). In other words,

$$\begin{aligned}
G(z, z') &= \phi_0 \left( \vec{b} - \vec{b}' \right) \int_{\epsilon-i\infty}^{\epsilon+i\infty} \frac{d\gamma}{2\pi i} e^{(z-z')\bar{\gamma}} \exp \left( (\gamma - \bar{\gamma}) (z - z') + \frac{1}{2} \omega''_{\gamma\bar{\gamma}} (\gamma = \gamma_{cr}, 0) Y (\gamma - \bar{\gamma})^2 \right) \\
&= \phi_0 \left( \vec{b} - \vec{b}' \right) e^{(z-z')\bar{\gamma}} \frac{1}{\sqrt{2\pi\omega''_{\gamma\bar{\gamma}} (\gamma = \gamma_{cr}, 0) (Y - Y')}} \exp \left( - \frac{(z - z')^2}{2\omega''_{\gamma\bar{\gamma}} (\gamma = \gamma_{cr}, 0) (Y - Y')} \right) \\
&\xrightarrow{z-z' \ll \sqrt{2\pi\omega''_{\gamma\bar{\gamma}} (\gamma = \gamma_{cr}, 0) (Y - Y')}} \frac{\phi_0 \left( \vec{b} - \vec{b}' \right)}{\sqrt{2\pi\omega''_{\gamma\bar{\gamma}} (\gamma = \gamma_{cr}, 0) (Y - Y')}} \left( \frac{r_1^2 Q_s^2(Y)}{r_2^2 Q_s^2(Y')} \right)^{\bar{\gamma}}
\end{aligned} \tag{3.24}$$

where  $Q_s^2(Y) = (1/R_p^2) \exp \left( \bar{\alpha}_S \frac{\chi(\gamma_{cr})}{\bar{\gamma}} Y \right)$  with  $R_p$  is the soft scale ( the size of the typical dipole in the proton).

One can see that Eq. (3.24) is very close to the solution in the toy model (see Eq. (3.12)). The main difference in the function  $\phi_0 \left( \vec{b} - \vec{b}' \right)$  since the factor  $1/\sqrt{2\pi\omega''_{\gamma\bar{\gamma}} (\gamma = \gamma_{cr}, 0) (Y - Y')}$  could be absorbed into the redefinition of the variable  $z$  [36, 37]. The origin of this factor is in the boundary condition:  $G(z, z' \rightarrow 0) \rightarrow N_{\mathcal{P}}(z)$ . In the vicinity of the saturation scale for the scattering with the nucleus  $N_{\mathcal{P}}(z)$  takes the following form

$$N_{\mathcal{P}}(z) = \phi_0 R_p^2 S_A(b) \left( r^2 Q_p^2(Y) \right)^{\bar{\gamma}} \tag{3.25}$$

with  $S_A(b)$  defined in Eq. (1.2).

Therefore,  $\phi_0 \left( \vec{b} - \vec{b}' \right) = \phi_0 R_p^2 S_A \left( \vec{b} - \vec{b}' \right)$  where  $\phi_0$  is a constant.

## 4. Enhanced diagrams: correlations in hadron-nucleus scattering

In this section we summarize the experience in the calculation of the first enhanced diagram and will discuss the A dependence of the correlation function for hadron-nucleus scattering.

First, we list the main features of the enhanced diagrams which we found instructive and which make our explicit calculation more transparent.

1. Each enhanced diagram has a Pomeron loop that starts at rapidity  $Y'$  with the Pomeron splitting and ends with the Pomeron merging at rapidity  $Y''$  (see Fig. 2). The first enhanced diagram has only one Pomeron loop . The calculation of the Pomeron loop in which Pomerons produce particles (see Fig. 2) turns out to be quite different from the calculation of the Pomeron loop in the total cross sections. The largest contributions of the Pomerons which propagate from rapidity  $Y'$  to rapidity



$Y''$  stems from the kinematic region in the vicinity of the saturation scale. This feature stems from the expression for single inclusive cross section that has been discussed in section 2.2 and is a manifestation that the typical transverse momenta of the gluons in the wave function of the fast hadron is about of the saturation scale  $Q_s$ .

2. Integration over the transverse momentum  $Q_T$  in the loop leads to the configuration with the same sizes of the dipoles at rapidity  $Y'$  and at rapidity  $Y''$  ( in the triple Pomeron vertices).
3. . In the integration over  $Q_T$  the value of the typical  $Q_T$  is the maximum of the saturation momenta for four Pomeron with the rapidities:  $(Y, Y')$  and  $(Y'', 0)$  (see Fig. 2).

$$Q_T \approx \max\left\{Q_s(Y - Y'), Q_s(Y''), \right\} \quad (4.1)$$

4. As we have discussed four Pomerons in the loop being in the vicinity of the saturation scale lead to the following rapidity dependence

$$\frac{d\sigma}{dY_1 dY_2 d^2p_{\perp,1} d^2p_{\perp,2}} \propto \exp\left(\chi(\bar{\gamma})((Y' - Y_1) + (Y_1 - Y'') + (Y - Y_2) + (Y_2 - Y''))\right) = \exp\left(2\chi(\bar{\gamma})(Y' - Y'')\right) \quad (4.2)$$

The maximal growth of the BFKL Pomerons with rapidities  $Y - Y'$  and  $Y''$  in the kinematic region far away of the saturation domain is given by

$$\exp\left(\chi(\gamma = 1/2)((Y - Y') + Y'')\right) \quad (4.3)$$

Collecting Eq. (4.2) and Eq. (4.3) we obtain

$$\frac{d\sigma}{dY_1 dY_2 d^2p_{\perp,1} d^2p_{\perp,2}} \propto \exp\left(2\chi(\bar{\gamma})(Y' - Y'') + \chi(\gamma = 1/2)((Y - Y') + Y'')\right) \quad (4.4)$$

Since  $2\chi(\bar{\gamma}) - \chi(\gamma = 1/2) > 0$  the integrals over  $Y'$  and  $Y''$  are convergent leading to  $Y' \rightarrow Y$  and  $Y'' \rightarrow 0$ . Therefore, the integration over  $Y'$  and  $Y''$  have the same structure as in calculation of the contribution of the enhanced diagram in the total cross section (see Ref. [43]).

5. For  $Y' = Y$  and  $Y'' = 0$  Eq. (4.1) takes the form:

$$Q_T = Q_s(A, Y = 0). \quad (4.5)$$

Actually we take into account Eq. (3.24) and Eq. (3.25) of the previous section to justify this equation.

Eq. (4.5) distinguishes the hadron-nucleus scattering from the hadron-hadron interaction and we need to re-consider the integration over  $R_1$  and  $R_2$  in Eq. (2.80) to take into account this equation. Re-visiting

this integration we see that Eq. (2.68) takes the form

$$\int d^2 p_{\perp,1} d^2 p_{\perp,2} \frac{d\sigma}{dY_1 dY_2 d^2 p_{\perp,1} d^2 p_{\perp,2}} = \quad (4.6)$$

$$N_0^2 \phi_0^4 \frac{8 C_F}{\alpha_s (2\pi)^4} \frac{8 C_F}{\alpha_s (2\pi)^4} \sigma_p \sigma_A \frac{1}{Q_s(A, Y=0)} Q_s^2(A; Y_1) Q_s^2(A; Y_2) \left( \frac{Q_s^2(p; Y - Y_1)}{Q_s^2(A; Y_1)} \right)^{2\bar{\gamma}}$$

where  $\sigma_p$  and  $\sigma_A$  are the cross sections of the interaction of the dipole with the typical size in a hadron with the hadron and nucleus, respectively. Plugging this equation in Eq. (2.69) we obtain that

$$R(A; Y_1, Y_2; Y) = \tilde{N}_0^2 I_Y(\bar{\gamma}) \frac{\sigma_{in}(Y)}{\sigma_A} \frac{1}{\sigma_p Q_s(A, Y=0)} \quad (4.7)$$

The factor  $\sigma_{in}(Y)/\sigma_A$  we will discuss below, but the ratio  $1/(\sigma_p Q_s(A, Y=0))$  was expected as the natural estimates for the correlations (see Ref. [23, 51]). However, in the angular correlations the extra factor  $Q_T^2$  appears in the integration over  $Q_T$  which leads to

$$R(\cos \varphi) = \frac{\frac{1}{\sigma_{in}} \int \frac{d\sigma}{dY_1 dY_2 d^2 p_{\perp,1} d^2 p_{\perp,2}} dp_{\perp,1}^2 dp_{\perp,1}^2}{\frac{1}{\sigma_{in}} \int \frac{d\sigma}{dY_1 d^2 p_{\perp,1}} dp_{\perp,1}^2 \frac{1}{\sigma_{in}} \int \frac{d\sigma}{dY_2 d^2 p_{\perp,1}} dp_{\perp,1}^2} = \cos^2 \varphi I(\bar{\gamma}) \tilde{N}_0^2 \frac{\sigma_{in}(Y)}{\sigma_A} \frac{Q_s(A, Y=0)}{Q_s(A, Y_1)} \frac{1}{\sigma_p Q_s(A, Y_2)} \quad (4.8)$$

where  $I(\bar{\gamma})$  is given by Eq. (2.84).

In the region of  $p_{1,\perp} \sim Q_s(A, Y_1)$  and  $p_{2,\perp} \sim Q_s(A, Y_2)$  the correlation function takes the form:

$$R(\cos \varphi, p_{\perp,1}, p_{\perp,2}) = \sigma_{in} \frac{\frac{d\sigma}{dY_1 dY_2 d^2 p_{\perp,1} d^2 p_{\perp,2}}}{\frac{d\sigma}{dY_1 d^2 p_{\perp,1}} \frac{d\sigma}{dY_2 d^2 p_{\perp,1}}} = \cos^2 \varphi I(\bar{\gamma}) \tilde{N}_0^2 \frac{\sigma_{in}(Y)}{\sigma_A} \frac{Q_s(A, Y=0)}{p_{1,\perp}^2} \frac{1}{\sigma_p p_{2,\perp}^2} \quad (4.9)$$

One can see that the contribution of the enhanced diagrams do not depend on  $\nabla^2 S_A(b)$  as in Eq. (1.1) and, therefore, the density variation mechanism, suggested in Ref. [24], does not lead to any suppression for the case of hadron-nucleus scattering.

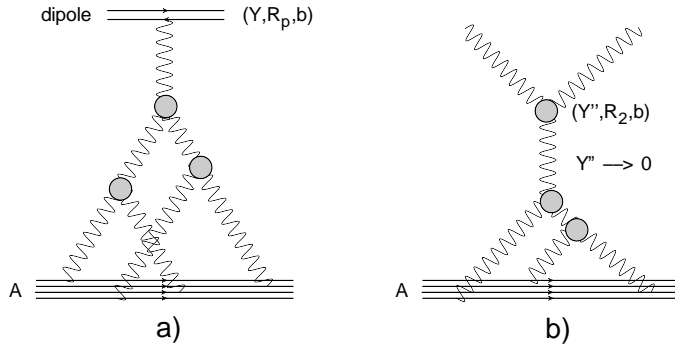


**Figure 16:**  $\sigma_{in}$  (see Fig. 16-a) and  $\tilde{N}_0$  (see Fig. 16-b) in Eq. (4.8).

In the definition of the correlation function in Eq. (4.8)  $\sigma_{in}(Y - Y_0)$  is the dipole-nucleus cross section shown in Fig. 16-a. From this figure one can see that  $\sigma_{in} = \int d^2b (2N_A(r, Y - Y_0; b) - N_A^2(r, Y - Y_0; b)) \propto A^{2/3}$  where  $N(r, Y; b)$  is the solution of the Balitsky-Kovchegov equation ( see Eq. (3.1) and Ref. [15]) with the initial condition given by the McLerran-Venugopalan formula [13]:

$$N_A(r, Y = Y_0; b) = 1 - \exp\left(-r^2 Q_A^2(Y = Y_0, b)/2\right) \quad \text{where} \quad Q_A^2(Y = Y_0, b) = Q_p^2(Y = Y_0) S_A(b) \quad (4.10)$$

with  $Q_p(Y = Y_0)$  is the saturation momentum of proton at low energy and  $S_A(b)$  is given by Eq. (1.2). It should be mentioned that we write the McLerran-Venugopalan formula for the inelastic cross section.

On the other hand  $N_0$  shown in Fig. 16-b is proportional to  $\int d^2b N_A(r, Y = 0; b) \propto A^{2/3}$  given by Eq. (4.10). Each factor in Eq. (4.8) is proportional to the ratio

$$\frac{\sigma_A}{\sigma_{in}} = \frac{\int d^2b N_A(r, Y = Y_0; b | \text{McLerran-Venugopalan formula})}{\int d^2b \left(2N_A^{\text{BK}}(r, Y - Y_0; b) - (N_A^{\text{BK}}(r, Y - Y_0; b))^2\right)} \quad (4.11)$$

This ration does not depend on  $A$  and it's value depends on the the value of  $Q_p^2(Y = Y_0)$  since the dominator in Eq. (4.11) is equal to  $\pi R_A^2$  where  $R_A$  is the nucleus radius. Only at ultra high energies the dominator of Eq. (4.11) starts depend on  $Y$  demonstrating the Froissart - type behaviour of the interaction radius. For  $Q_p^2(Y = Y_0) = 0.2 \text{ GeV}^2$  we obtain  $\sigma_{in}(Y - Y_0)/\sigma_A \approx 14.5$  at  $W = 5.5 \text{ TeV}$  for gold.  $R^2$  in Eq. (4.8) is the size of the dipole in the proton, which is found to be about  $1/\text{GeV}^2$  in Ref. [49]. It gives  $R(\cos \varphi) = 1.45 \cos^2 \varphi (Q_s(A, Y = 0)/Q_s(A, Y_1)) (1/(\sigma_p Q_s(A, Y_2)))$ . In other words

$$\frac{R_A(\cos \varphi, p_{\perp,1}, p_{\perp,2})}{R_p(\cos \varphi, p_{\perp,1}, p_{\perp,2})} \approx 2 \frac{\sigma_p}{\sigma_{in}(Y)} R_p^2 Q_s^2(A, Y = 0) \approx (0.8 \div 1) A^{1/3} \leftarrow \text{at LHC energy} \quad (4.12)$$

In Eq. (4.12) we denote by  $R_A$  the correlation function of Eq. (4.9) and by  $R_p$  the correlation function of Eq. (2.85).

## 5. Conclusions

As it has been mentioned the main goal of this paper is to developed a more quantitative approach for the density variation mechanism suggested in Ref. [24]. Calculating the first BFKL Pomeron loop diagrams in the dense parton environment in which the density variations have been expected to be large, we learned the following lessons.

First, the calculation of the enhanced diagram for the double inclusive productions shows the same pattern as for the total cross section:  $Y' \rightarrow Y$  and  $Y'' \rightarrow 0$  where  $Y'$  and  $Y''$  are rapidities of the upper and low vertices, respectively.

Second, the correlation function generated by this diagram turns out to be large , viz,

$$R(Y_1, Y_2; Y) = \frac{\frac{1}{\sigma_{in}(Y)} \int d^2p_{1,T} d^2p_{2,T} \frac{d^2\sigma}{dY_1 d^2p_{1,T} dY_2 d^2p_{2,T}}}{\frac{1}{\sigma_{in}(Y)} \int d^2p_{1,T} \frac{d^2\sigma}{dY_1 d^2p_{1,T}} \frac{1}{\sigma_{in}(Y)} \int d^2p_{1,T} \frac{d^2\sigma}{dY_1 d^2p_{1,T}}} - 1 \propto \frac{\sigma_{in}(Y)}{\pi R^2} \quad (5.1)$$

where  $R$  is the size of the typical dipole inside the proton.

In Eq. (5.1)  $\sigma_{in} = \sigma_{tot} - \sigma_{el} - \sigma_{sd} - \sigma_{dd}$  where  $\sigma_{el}, \sigma_{sd}$  and  $\sigma_{dd}$  are cross section for elastic scattering and single and double diffractive production. All rapidities are denoted in Fig. 2. This estimate looks natural since  $1/R^2$  is the typical momentum in the Pomeron loop in Fig. 2 and  $\sigma_{in}$  stems from the definition of  $R(Y_1, Y_2, Y)$ . The production of the gluon jet by the Pomerons in the loop cancel with the dominators in Eq. (5.1).

Third, the azimuthal correlations induced by the enhanced Pomeron diagram, are suppressed in comparison with the rapidity correlations by factor  $0.53 / (2(1 + 2\gamma_{cr}))^2 \approx 0.045 / (R^2 Q_s(Y_1) R^2 Q_s(Y_1))$ .

Fourth, it turns out the the typical sizes of dipoles in two triple Pomeron vertices in the Pomeron loop are the same and they are both of the order of the size of the typical dipole inside the proton  $R$ .

The main observation of the papers that the correlations generated by the enhanced diagrams depend on the processes, in which they are measured. In particular, the rapidity correlations for the hadron-nucleus collisions take the following form:

$$R(A; Y_1, Y_2; Y) \propto \frac{1}{\sigma_p Q_s(A, Y=0)} \propto 1/A^{1/3} \quad (5.2)$$

The suppression of the angular correlations turns out to be more pronounced, viz.

$$\frac{R(\cos \varphi; pA)}{R(\cos \varphi; pp)} \propto A^{-1/3} \quad (5.3)$$

In general the enhanced diagrams generate rather small angular correlation functions but the coefficient in front of  $\cos^2 \varphi$  turns out to be rather large. The smallness of the correlation function stems from the large values of the single inclusive cross section which is proportional to the multiplicity of produced gluons. In particular, for hadron-nucleus collisions

$$\int d^2 p_{\perp,1} d^2 p_{\perp,2} \frac{d\sigma(pA)}{dY_1 dY_2 d^2 p_{\perp,1} d^2 p_{\perp,2}} \propto \cos^2 \varphi A^{1/3} \quad (5.4)$$

Eq. (5.4) is most pronounced in the ratio

$$\frac{R_A(\cos \varphi, p_{\perp,1}, p_{\perp,2})}{R_p(\cos \varphi, p_{\perp,1}, p_{\perp,2})} \propto A^{1/3} \quad (5.5)$$

In general we demonstrate that the density variation mechanism suggested in Ref. [24] generates sizable contributions to the coefficient in front of  $\cos^2 \varphi$  in the double inclusive cross sections. The value of this coefficient is proportional  $A^{1/3}$ , does not include  $\nabla^2 S_A(b)$  as in Eq. (1.1) and, therefore, density variation mechanism leads to substantial contribution for hadron-nucleus collision.

## 6. Acknowledgements

We thank our colleagues at UTFSM and Tel Aviv university for encouraging discussions. This research was supported by the BSF grant 2012124 and by the Fondecyt (Chile) grants 1140842 and 1120920.

## References

- [1] V. Khachatryan *et al.* [CMS Collaboration], *JHEP* **1009** (2010) 091 [arXiv:1009.4122 [hep-ex]].
- [2] J. Adams *et al.* [STAR Collaboration], *Phys. Rev. Lett.* **95** (2005) 152301 [nucl-ex/0501016].
- [3] B. Alver *et al.* [PHOBOS Collaboration], *Phys. Rev. Lett.* **104** (2010) 062301 [arXiv:0903.2811 [nucl-ex]].
- [4] H. Agakishiev *et al.* [STAR Collaboration], arXiv:1010.0690 [nucl-ex].
- [5] S. Chatrchyan *et al.* [CMS Collaboration], *Phys. Lett. B* **718** (2013) 795 [arXiv:1210.5482 [nucl-ex]].
- [6] S. Chatrchyan *et al.* [CMS Collaboration], *Eur. Phys. J. C* **72** (2012) 2012 [arXiv:1201.3158 [nucl-ex]].
- [7] A. R. Timmins [ALICE Collaboration], *J. Phys. G* **38** (2011) 124093; A. R. Timmins [ALICE Collaboration], arXiv:1106.6057 [nucl-ex]; *J. Phys. G* **38** (2011) 124091 [arXiv:1107.0285 [nucl-ex]].
- [8] A. Dumitru, F. Gelis, L. McLerran and R. Venugopalan, *Nucl. Phys. A* **810** (2008) 91 [arXiv:0804.3858 [hep-ph]].
- [9] E. A. Kuraev, L. N. Lipatov, and F. S. Fadin, *Sov. Phys. JETP* **45**, 199 (1977); Ya. Ya. Balitsky and L. N. Lipatov, *Sov. J. Nucl. Phys.* **28**, 822 (1978).
- [10] L. N. Lipatov, *Phys. Rep.* **286** (1997) 131; *Sov. Phys. JETP* **63** (1986) 904 [*Zh. Eksp. Teor. Fiz.* **90**, 1536 (1986)].
- [11] L. V. Gribov, E. M. Levin and M. G. Ryskin, *Phys. Rep.* **100** (1983) 1.
- [12] A. H. Mueller and J. Qiu, *Nucl. Phys.* **B268** (1986) 427.
- [13] L. McLerran and R. Venugopalan, *Phys. Rev.* **D49** (1994) 2233, 3352; **D50** (1994) 2225; **D53** (1996) 458; **D59** (1999) 09400.
- [14] A. H. Mueller, *Nucl. Phys. B* **415**, 373 (1994); *Nucl. Phys. B* **437** (1995) 107 [arXiv:hep-ph/9408245].
- [15] I. Balitsky, [arXiv:hep-ph/9509348]; *Phys. Rev.* **D60**, 014020 (1999) [arXiv:hep-ph/9812311] Y. V. Kovchegov, *Phys. Rev.* **D60**, 034008 (1999), [arXiv:hep-ph/9901281].
- [16] J. Jalilian-Marian, A. Kovner, A. Leonidov and H. Weigert, *Phys. Rev.* **D59**, 014014 (1999), [arXiv:hep-ph/9706377]; *Nucl. Phys.* **B504**, 415 (1997), [arXiv:hep-ph/9701284]; J. Jalilian-Marian, A. Kovner and H. Weigert, *Phys. Rev.* **D59**, 014015 (1999), [arXiv:hep-ph/9709432]; A. Kovner, J. G. Milhano and H. Weigert, *Phys. Rev.* **D62**, 114005 (2000), [arXiv:hep-ph/0004014]; E. Iancu, A. Leonidov and L. D. McLerran, *Phys. Lett.* **B510**, 133 (2001); [arXiv:hep-ph/0102009]; *Nucl. Phys.* **A692**, 583 (2001), [arXiv:hep-ph/0011241]; E. Ferreira, E. Iancu, A. Leonidov and L. McLerran, *Nucl. Phys.* **A703**, 489 (2002), [arXiv:hep-ph/0109115]; H. Weigert, *Nucl. Phys.* **A703**, 823 (2002), [arXiv:hep-ph/0004044].
- [17] Yuri V Kovchegov and Eugene Levin, “*Quantum Chromodynamics at High Energies*”, Cambridge Monographs on Particle Physics, Nuclear Physics and Cosmology, Cambridge University Press, 2012 and references therein.
- [18] T. Altinoluk, A. Kovner, E. Levin and M. Lublinsky, “*Reggeon Field Theory for Large Pomeron Loops*,” arXiv:1401.7431 [hep-ph] and references therein.
- [19] E. V. Shuryak, *Phys. Rev. C* **76** (2007) 047901 [arXiv:0706.3531 [nucl-th]]; S. A. Voloshin, *Phys. Lett. B* **632** (2006) 490 [nucl-th/0312065]; S. Gavin, L. McLerran and G. Moschelli, *Phys. Rev. C* **79** (2009) 051902 [arXiv:0806.4718 [nucl-th]].

- [20] A. Kovner, “*How to build a ridge in pA collisions*”, talk at Low x WS, May 30 - June 4, 2013, Rehovot-Eilat, Israel. <http://www.weizmann.ac.il/MaKaC/getFile.py/access?contribId=60&sessionId=25&resId=0&materialId=slides&confId=16>
- [21] A. Dumitru, K. Dusling, F. Gelis, J. Jalilian-Marian, T. Lappi and R. Venugopalan, Phys. Lett. B **697** (2011) 21 [arXiv:1009.5295 [hep-ph]].
- [22] A. Kovner and M. Lublinsky, Phys. Rev. D **83** (2011) 034017 [arXiv:1012.3398 [hep-ph]].
- [23] A. Kovner and M. Lublinsky, Int. J. Mod. Phys. E **22** (2013) 1330001 [arXiv:1211.1928 [hep-ph]].
- [24] E. Levin and A. H. Rezaeian, Phys. Rev. D **84**, 034031 (2011) [arXiv:1105.3275 [hep-ph]].
- [25] R. L. Ray, “*Azimuthal quadrupole correlation from gluon interference in 200 GeV p+p collisions*,” arXiv:1406.2736 [hep-ph].
- [26] W. Li, Mod. Phys. Lett. A **27** (2012) 1230018 [arXiv:1206.0148 [nucl-ex]].
- [27] A. Kovner, Acta Phys. Polon. B **42** (2011) 2717.
- [28] C. J. Horowitz, Int. J. Mod. Phys. E **20** (2011) 1 [arXiv:1106.1661 [astro-ph.SR]].
- [29] T. Lappi, Int. J. Mod. Phys. E **20** (2011) 1 [arXiv:1003.1852 [hep-ph]].
- [30] E. Iancu, arXiv:1205.0579 [hep-ph].
- [31] R. Venugopalan, PoS QNP **2012** (2012) 019 [arXiv:1208.5731 [hep-ph]].
- [32] A. H. Mueller, Phys. Rev. D **2** (1970) 2963.
- [33] H. Navelet and R. B. Peschanski, Nucl. Phys. B **507**, 35 (1997) [hep-ph/9703238]; Phys. Rev. Lett. **82** (1999) 1370 [hep-ph/9809474]; Nucl. Phys. B **634** (2002) 291 [hep-ph/0201285].
- [34] I. Gradshteyn and I. Ryzhik, *Table of Integrals, Series, and Products*, Fifth Edition, Academic Press, London, 1994.
- [35] M. Braun, Eur. Phys. J. C **16**, 337 (2000) [hep-ph/0001268]; Phys. Lett. B **483** (2000) 115, [arXiv:hep-ph/0003004]; Eur. Phys. J. C **33** (2004) 113 [arXiv:hep-ph/0309293]; Phys. Lett. B **632** (2006) 297, [Eur. Phys. J. C **48** (2006) 511], [arXiv:hep-ph/0512057].
- [36] A. H. Mueller and D. N. Triantafyllopoulos, Nucl. Phys. B **640** (2002) 331 [arXiv:hep-ph/0205167]; D. N. Triantafyllopoulos, Nucl. Phys. B **648** (2003) 293 [arXiv:hep-ph/0209121].
- [37] S. Munier and R. B. Peschanski, Phys. Rev. D **70** (2004) 077503 [arXiv:hep-ph/0401215]; Phys. Rev. D **69** (2004) 034008 [arXiv:hep-ph/0310357]; Phys. Rev. Lett. **91** (2003) 232001 [arXiv:hep-ph/0309177].
- [38] E. Iancu, K. Itakura, L. McLerran, Nucl. Phys. A **708** (2002) 327. [hep-ph/0203137]
- [39] E. Iancu, K. Itakura and S. Munier, Phys. Lett. B **590**, 199 (2004) [hep-ph/0310338].
- [40] S. Catani, M. Ciafaloni and F. Hautmann, Nucl. Phys. B **366** (1991) 135; Nucl. Phys. Proc. Suppl. **29A** (1992) 182; J. C. Collins and R. K. Ellis, Nucl. Phys. B **360** (1991) 3; E. M. Levin, M. G. Ryskin, Y. M. Shabelski and A. G. Shuvaev, Sov. J. Nucl. Phys. **53** (1991) 657 [Yad. Fiz. **53** (1991) 1059].
- [41] Y. V. Kovchegov and K. Tuchin, Phys. Rev. D **65** (2002) 074026 [arXiv:hep-ph/0111362].
- [42] J. Jalilian-Marian and Y. V. Kovchegov, Phys. Rev. D **70** (2004) 114017 [Erratum-ibid. D **71** (2005) 079901] [hep-ph/0405266]; Prog. Part. Nucl. Phys. **56** (2006) 104 [hep-ph/0505052].

- [43] E. Levin, J. Miller and A. Prygarin, Nucl. Phys. A **806**, 245 (2008) [arXiv:0706.2944 [hep-ph]].
- [44] E. Levin and M. Lublinsky, Nucl. Phys. A **730**, 191 (2004) [hep-ph/0308279]; Phys. Lett. B **607** (2005) 131 [hep-ph/0411121].
- [45] I. N. Sneddon, Elements of partial differential equations, Mc-Graw-Hill, New York, 1957.
- [46] J. Bartels, E. Levin, Nucl. Phys. **B387** (1992) 617-637; A. M. Stasto, K. J. Golec-Biernat, J. Kwiecinski, Phys. Rev. Lett. **86** (2001) 596-599, [hep-ph/0007192]; L. McLerran, M. Praszalowicz, Acta Phys. Polon. **B42** (2011) 99, [arXiv:1011.3403 [hep-ph]] **B41** (2010) 1917-1926, [arXiv:1006.4293 [hep-ph]]. M. Praszalowicz, [arXiv:1104.1777 [hep-ph]], [arXiv:1101.0585 [hep-ph]].
- [47] E. Levin and K. Tuchin, Nucl. Phys. B **573** (2000) 833 [arXiv:hep-ph/9908317].
- [48] A. H. Mueller and A. I. Shoshi, Nucl. Phys. B **692** (2004) 175 [arXiv:hep-ph/0402193].
- [49] E. Levin, JHEP **1311**, 039 (2013) [arXiv:1308.5052 [hep-ph]].
- [50] D. Kharzeev and M. Nardi, Phys. Lett. **B 507** (2001) 121; D. Kharzeev and E. Levin, Phys. Lett. **B 523** (2001) 79; D. Kharzeev, E. Levin and M. Nardi, Phys. Rev. C **71**, 054903 (2005) [hep-ph/0111315]; Nucl. Phys. A **747**, 609 (2005) [hep-ph/0408050]; D. Kharzeev, E. Levin and L. McLerran, Phys. Lett. B **561** (2003) 93; A. Dumitru, D. E. Kharzeev, E. M. Levin and Y. Nara, Phys. Rev. C **85**, 044920 (2012) [arXiv:1111.3031 [hep-ph]].
- [51] K. Dusling, F. Gelis, T. Lappi and R. Venugopalan, Nucl. Phys. A **836**, 159 (2010), F. Gelis, T. Lappi and R. Venugopalan, Nucl. Phys. A **830**, 591C (2009).